DOI: 10.1002/anie.201405910

Energy Materials

# Energy Storage Materials Synthesized from Ionic Liquids

*Gebrekidan Gebresilassie Eshetu, Michel Armand, Bruno Scrosati,* and Stefano Passerini**

**Keywords:**
batteries · energy storage · ionic liquids · super capacitors · synthesis

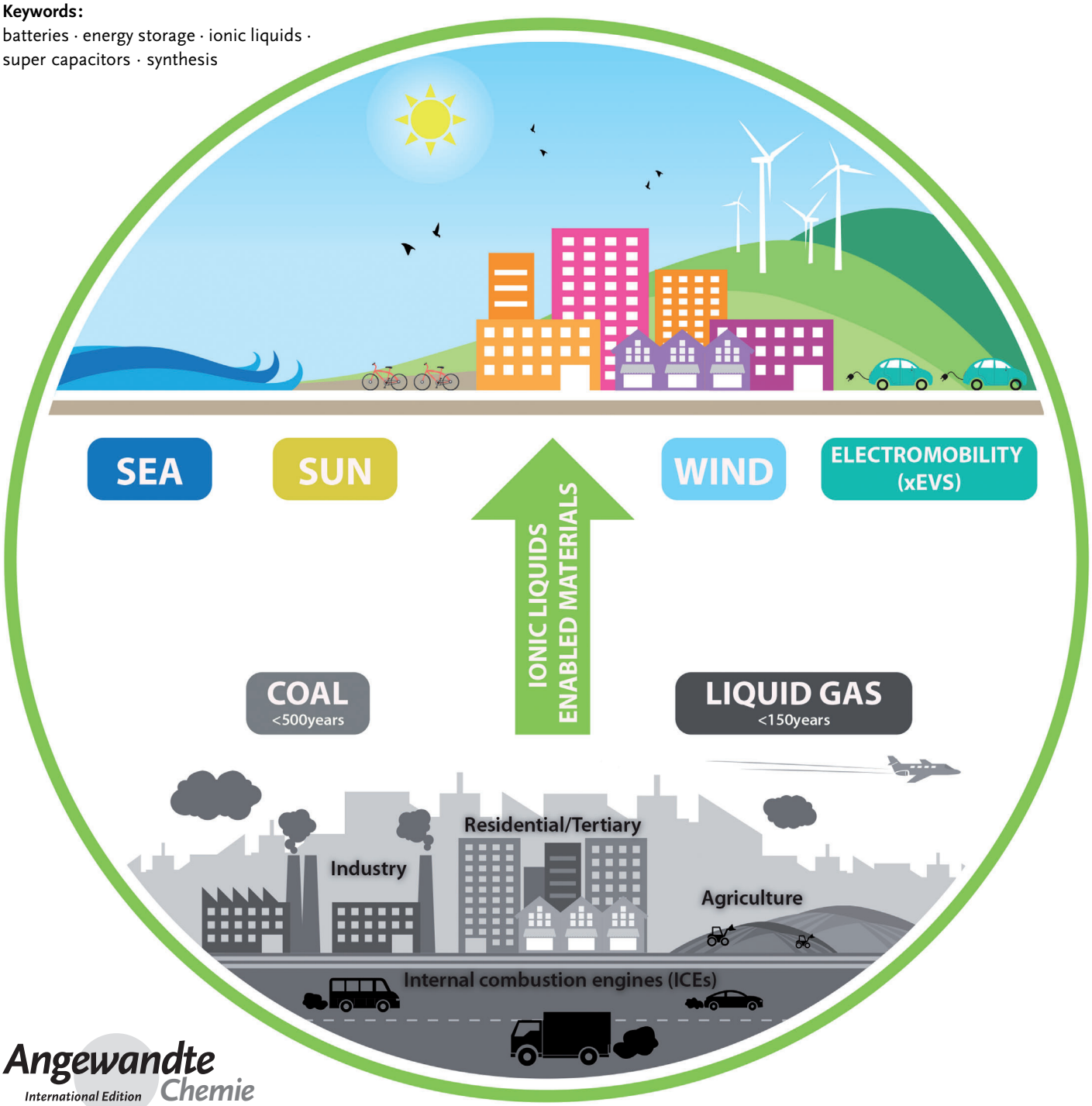

*The advent of ionic liquids (ILs) as eco-friendly and promising reaction media has opened new frontiers in the field of electrochemical energy storage. Beyond their use as electrolyte components in batteries and supercapacitors, ILs have unique properties that make them suitable as functional advanced materials, media for materials production, and components for preparing highly engineered functional products. Aiming at offering an in-depth review on the newly emerging IL-based green synthesis processes of energy storage materials, this Review provides an overview of the role of ILs in the synthesis of materials for batteries, supercapacitors, and green electrode processing. It is expected that this Review will assess the status quo of the research field and thereby stimulate new thoughts and ideas on the emerging challenges and opportunities of IL-based syntheses of energy materials.*

**From the Contents**



## 1. Introduction

Environmental concerns regarding the use of fossil fuels and their resource constraints, combined with energy security fears, have spurred an increasingly urgent and strategic development of alternative approaches toward energy production, storage and delivery. These alarming concerns are raising the consideration of renewable energy sources (such as solar power and wind) for the replacement of the oil-based energy generation systems. However, though these readily available green energy sources have the potential to reduce our dependence on the limited fossil fuel supply, while concomitantly ensuring both climate and energy securities, they are difficult to use for base-load power generation as their outputs are very volatile and heavily depend on their instantaneous availability. To smooth out the intermittency of such technologies and thereby ensure the balance between energy demand and supply, the -discovery and application of new materials that offer significant improvements in the way that energy is produced, stored, and delivered is of paramount importance.[1,2] In this regard, ionic liquids (ILs) are one such class of novel and propitious materials that are attracting attention for a broad range of applications. In fact, they offer a range of properties that can be tuned to optimize their roles in multifarious applications. Ionic liquids can be regarded as a family of room-temperature molten salts, composed entirely of ions that undergo almost unlimited structural variations through appropriate modification of the cations and anions.[3–5]

Over the past decade, ILs have become one of the fastest growing "green" media due to their peculiar physicochemical properties such as nearly-zero vapor pressure, good thermal stability, wide liquid range, tunable solubility of both organic and inorganic molecules, and broad electrochemical window. The highly flexible synthesis of these materials favors the introduction of specific features for a given application, such as hydrophobicity versus hydrophilicity and the possibility to add functional groups for reactivity purposes, among many others.[6,7]

Figure 1 presents a list of representative cations/anions of ionic liquids and their peculiar characteristics from the materials synthesis perspective. These peculiar properties endow ILs as reaction media in the synthesis of inorganic materials as advanced functional solvents, structure-directing and -inducing agents, charge-compensating groups, and precursors, resulting in products with special structures, morphologies, and properties in a controlled and tunable manner, which could otherwise be difficult or impossible to obtain with other conventional methods such as solid-state reaction, hydro- or solvothermal synthesis, and others. Additionally, their indefinite recyclability frequently compensates for the elevated cost of ionic liquids, which is considered as a major drawback of these solvents. For most applications ILs can, after appropriate purification, be reused indefinitely without any noticeable difference in the quality of the resulting products.

As witnessed by the emergence of thousands of publications, ionic liquids span over a wide range of applications, serving as electrolytes in energy storage (e.g., batteries and supercapacitors) and conversion devices (solar cells and fuel cells), for catalysis, separation, as tailor-made lubricants, and also as all-in-one reaction media in organic and/or inorganic synthesis, to name only a few.

Besides their successful application in the synthesis of conventional inorganic materials, ILs have recently attracted

[*] Dr. G. Gebresilassie Eshetu, Prof. Dr. S. Passerini
Helmholtz Institute Ulm (HIU), Electrochemical Energy Storage
Helmholtz Strasse 11, 89081 Ulm (Germany)
E-mail: Stefano.passerini@kit.edu
Dr. G. Gebresilassie Eshetu, Prof. Dr. S. Passerini
Karlsruhe Institute of Technology (KIT)
P.O. Box 3640, 76021 Karlsruhe (Germany)
Prof. Dr. B. Scrosati
Italian Institute of Technology
Genova (Italy)
E-mail: bruno.scrosati@gmail.com
Prof. Dr. M. Armand
CIC Energigune, Parque Tecnologico de Alava
Albert Einsten, 48, ED. CIC, 01510 Miñano (Spain)

  

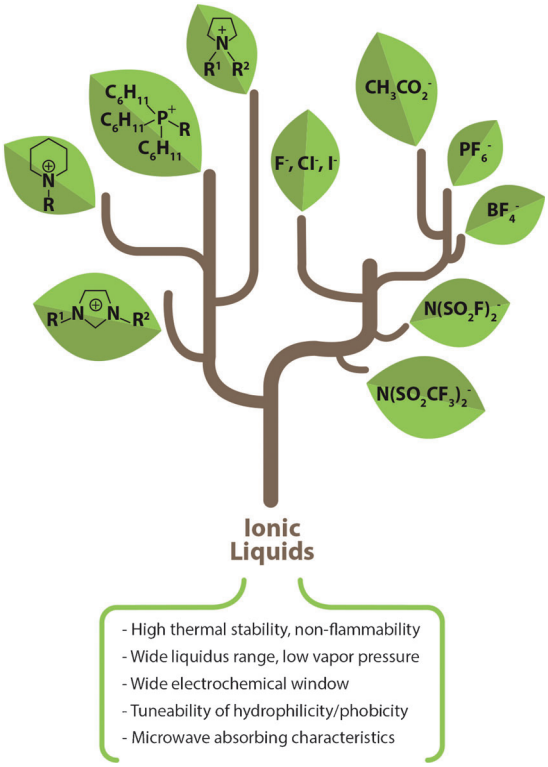


***Figure 1.*** Representative cations/anions of ILs along with their beneficial characteristics.

the attention of the energy materials community because they offer unprecedented opportunities for materials synthesis. In fact, they could in principle be used in any situation in which the hydro- or solvothermal synthesis routes have been successfully implemented. The large temperature window of ILs offers more environmentally friendly and safer reaction media, and the negligible vapor pressure avoids the need to work with autoclaves.

The wide electrochemical window of ILs enables the electrodeposition of reducing metals or semiconductors that previously could not be deposited from conventional water baths. The current trends in the material synthesis are also pointing to synergistic approaches such as microwave- (MW-IL) and ultrasound-assisted synthesis routes in IL media toward obtaining novel materials. In fact, owing to the excellent absorbing characteristics of ILs, microwave-enhanced ionothermal synthesis, leading to a rapid crystal-growth rate and high product selectivity, can be effectively exploited.

Although there is a considerable number of stimulating short accounts focused on the general use of ILs in the inorganic materials synthesis, a comprehensive and updated review on the use of ILs for the energy materials synthesis is still lacking, especially considering the fast growth of the field. In fact, even if the use of $AlCl_4^-$ and $Al_2Cl_7^-$ based ILs for the reforming of hydrocarbons is ignored, a rapidly growing number of scientific publications are appearing (Figure 2).

*Dr. Gebrekidan Gebresilassie Eshetu earned his M.Sc. in Materials Science and Chemical Engineering, under the Erasmus Mundus (European Union) scholarship program, from the European universities: UPJV (France), WUT (Poland), UPS (France), UCO (Spain), and AMU (France). He did his master thesis with Prof. Thierry Brousse on pseudocapacitor materials. He received his Ph.D in Materials Science in 2013, working with Prof. S. Laruelle, Prof. M. Armand, Dr. S. Grugeon (LRCS), and Dr. G. Marlair (INERIS) from UPJV (France). He is currently doing his postdoctoral research at the Helmholtz Institute of Ulm of the Karlsruhe Institute of Technology (KIT), Germany. His research focuses on electrochemical energy storage technologies.*

*Prof. Dr. Michel Armand was educated in France and USA; Ph.D. in Physics (1978); Fullbright Fellow, Directeur de Recherche at CNRS; invited scholar, Lawrence Berkeley Laboratory (1982–1983). Director of the Joint CNRS-University of Montreal International Laboratory (1995–2004). "Thinker in Residence", Deakin University 2013–2014. Now sharing his time between CNRS in France and CIC Energigune in Spain. He has brought forward several concepts for energy-related electrochemistry: intercalation compounds, polymer electrolytes, highly conductive salts for liquids, polymer electrolytes, and ionic liquids. His carbon "nanopainting" process has made $LiFePO_4$@C a safe, widely used cathode.*

*Prof. Dr. Bruno Scrosati, formerly Full Professor at the University of Rome La Sapienza, is presently affiliated with the Italian Institute of Technology in Genova, Italy. He received honorary doctorates from St. Andrews (Scotland), Chalmers (Sweden), and Ulm (Germany) universities, the Research Award from the Battery Division of the Electrochemical Society, the XVI Edition of the Italgas Prize, and the Vittorio de Nora award of the Electrochemical Society. He has been President of the Italian Chemical Society and the Electrochemical Society as well as European Editor of the Journal of Power Sources.*

*Prof. Dr. Stefano Passerini is a Professor at the Karlsruhe Institute of Technology (KIT), Helmholtz Institute Ulm. Formerly Professor at the University of Muenster, he co-founded the MEET battery research center. His research activities focus on electrochemical energy storage in batteries and supercapacitors. He has been awarded the Research Award of the Electrochemical Society Battery Division in 2012. Since 2013, he is the European Editor of the Journal of Power Sources.*

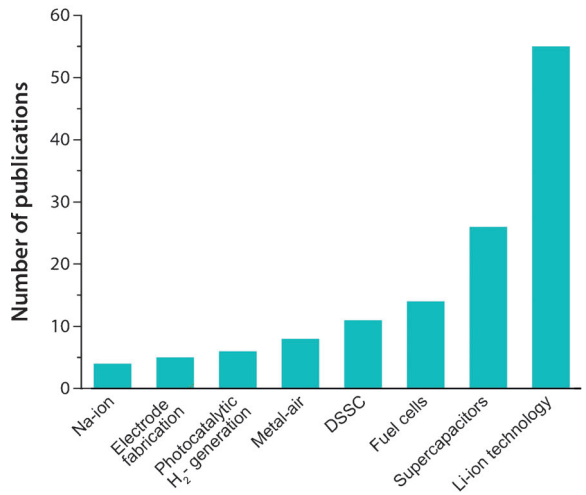


***Figure 2.*** Overall number of citations on SciFinder/Scopus/WebScience regarding the use of ILs for the synthesis of energy materials, up to May 2014.

In this Review the most recent progress in the synthesis of energy storage materials, more specifically those used for batteries (Li-ion, metal-air, and Na-ion) and supercapacitors, as well as in the development of eco-friendly electrode fabrication processes are discussed and evaluated. Finally, we critically assess the current status quo of the research field and put forward our own perspectives on future research directions.

For the sake of convenience for our readers, the acronyms along with the description of the ionic liquids used in this review are provided in Table 1.

## 2. The Use of ILs for the Synthesis of Energy Storage Systems

The strongest motivation for the development of ionic liquids in the electrochemical energy storage field was related to their use as functional electrolytes.[4,5] However, recently, ILs also have a significant impact as reaction media, precursors, and efficient structure-directing (capping) agents in the design of tailored electrode materials, current collectors, ceramic electrolytes, electrocatalysts, and in electrode-producing processes. The purpose of this section is to present the evolution of the IL-based preparation method in the fabrication of electroactive and -inactive materials, which are novel or offer better performance than the existing ones.

### 2.1. Lithium-Ion Batteries

Li-ion battery (LIB) technology, which has revolutionized the portable and hand-held devices market, is on the verge of penetrating into xEVs (pure electric vehicles (EVs) and (plug-in) hybrids) market upon the conditions that improvements can be achieved in terms of safety, cost and performance. Conceivably, high energy, long-term stability, safety, and low cost appear to be the overriding factors for large-scale applications, such as in the electromobility and grid/utility-storage systems. This in turn implies assessing the present materials used in these electrical energy storage systems and their synthetic routes, to define the challenges. In this subsection, a comprehensive Review on the major research progress in the synthesis of Li-ion battery components such as electrodes, electrolytes, and current collectors by the ionothermal synthesis route will be discussed.

#### 2.1.1. Electrode Materials

To meet the future challenges of LIBs, the discovery of new electrode materials, and/or the finding of new ways to

***Table 1:*** Inclusive list of acronyms and descriptions of ILs used in this Review.

| Acronyms | Ionic liquid |
|---|---|
| $[C_4mim][HSO_4]$ | 1-butyl-3-methylimidazolium bisulfate |
| $[C_nmim][Br]$ | 1-alkyl-3-methylimidazolium bromide |
| $[C_{16}mim][Cl]$ | 1-hexadecyl-3-methylimidazolium chloride |
| $[C_8mim][Cl]$ | 1-octyl-3-methylimidazolium chloride |
| $[C_4mim][BF_4]$ | 1-butyl-3-methylimidazolium tetrafluoroborate |
| $[C_8mim][BF_4]$ | 1-octyl-3-methylimidazolium tetrafluoroborate |
| $[C_2mim][Tf_2N]$ | 1-ethyl-3-methylimidazolium bis(tri-fluoromethanesulfonyl)imide |
| $[C_4mim][Cl]$ | 1-butyl-3-methylimidazolium chloride |
| $[C_6mim][FeCl_4]$ | 1-hexyl-3-methylimidazolium tetrachloroferrate(III) |
| $[C_3mim][I]$ | 1-propyl-3-methylimidazolium iodide |
| $[C_2mim][OTf]$ | 1-ethyl-3-methylimidazolium trifluoromethanesulfonate |
| $[C_nmim][Tf]$ | 1-alkyl-3-methylimidazolium triflate |
| $[C_2mim][OAc]$ | 1-ethyl-3-methylimidazolium acetate |
| ([Pyr14][$Tf_2N$] or [$C_4mpy$][$Tf_2N$]) | *N*-butyl-*N*-methylpyrrolidinium bis(trifluoromethanesulfonyl)amide |
| $[C_2mim][BF_4]$ | 1-ethyl-3-methylimidazolium tetrafluoroborate |
| $[C_{12}mim][Br]$ | 1-dodecyl-3-methylimidazolium bromide |
| $[C_8mim][Tf_2N]$ | 1-octyl-3-methylimidazolium bis(tri-fluoromethanesulfonyl)imide |
| $[C_{16}mim][Tf_2N]$ | 1-hexadecyl-3-methylimidazolium bis(tri-fluoromethanesulfonyl)imide |
| $[C_2mim][Cl]$ | 1-ethyl-3-methylimidazolium chloride |
| [(3-aminopropyl)mim][Br] | 1-(3-aminopropyl)-3-methylimidazolium bromide |
| $[P_{66614}][Tf_2N]$ | trihexyl(tetradecyl)phosphonium bis(trifluoromethanesulfonyl)imide |
| $[C_4(2\text{-}C_1)mim][Tf_2N]$ | 1,2-dimethyl-3-butylimidazolium bis(trifluoromethanesulfonyl)amide |
| $[C_4mim][N(CN)_2]$ | 1-butyl-3-methylimidazolium dicyanamide |
| $[C_{16}mim][BF_4]$ | 1-hexadecyl-3-methylimidazolium tetrafluoroborate |
| $[C_4mim][PF_6]$ | 1-butyl-3-methylimidazolium hexafluorophosphate |
| $[C_4mim][Tf_2N]$ | 1-butyl-3-methylimidazolium bis(trifluoromethanesulfonyl)imide |
| $[C_4C_1Pyr][Tf_2N]$ | 1-butyl-1-methylpyrrolidinium bis(trifluoromethanesulfonyl)imide |
| $[C_4mim][FeCl_4]$ | 1-butyl-3-methylimidazolium tetrachloroferrate(III) |
| $[C_2mim][Br]$ | 1-ethyl-3-methylimidazolium bromide |
| $[C_{16}mim][Br]$ | 1-hexadecyl-3-methylimidazolium bromide |
| $C_2$-OH | 1,2-dimethyl-3-(3-hydroxypropyl)imidazolium bis(trifluoromethanesulfonyl)imide |

synthesize known materials with tailored properties is of paramount importance. Recently, IL-assisted processes have appeared very appealing for the synthesis of highly engineered electrode materials at significantly lower temperatures. The versatility and richness of ionothermal synthesis, its control over particle size and shape, and the ability to provide stabilization to new phases are among the peculiar benefits offered by ILs. Henceforth, this section of the manuscript presents the progress made in the production of new or enhanced anode and cathode electrode materials by IL-assisted synthesis methods.

*Anode Materials*

Overcoming the safety issues related with the dendrite growth on lithium metal anodes, graphite host materials have been the key players in the commercial development of lithium-ion batteries. Graphite-based anode materials have long cycle life and low cost. However, these benefits are compromised when being sought for high-energy and power-intensive applications. Aware of these limitations, researchers are focusing on the modification of existing materials and/or the design of new electrode materials. With regard to the former approach, the doping of carbonaceous materials with heteroatoms such as N, S, and B has been investigated, aiming at fine-tuning the physicochemical properties of carbon materials and thereby effectively improving both the electronic conductivity and the electroactivity versus lithium. Combining the advantages of liquid state and negligible vapor pressure, ILs are almost ideal precursors for the N- and S-doping/co-doping of carbon materials, allowing simple processing and shaping as compared to solid and, even more, gas-phase reactions.[8] Yan et al.[9] reported the preparation of S-doped porous carbon hybridized with graphene (SPC@G) using $[C_4mim][HSO_4]$ both as a stabilizer for graphene and a sacrificial soft template. Whilst the hierarchical porous carbon facilitates the abundant absorption of $Li^+$ ions by SPC@G, the S-doped porous carbon uniformly embedded within graphene increases the number of nanopores, the interlayer distance along the $d_{002}$ direction, and the electronic conductivity. The combined structural features endowed the SPC@G with ultrahigh reversible capacity, long cycle life, and excellent power performance. Similarly, nitrogen and oxygen co-doped porous carbon nanobubbles fabricated by using a silica-templated ionic liquid ($C_n$mimBr) impregnation method showed enhanced $Li^+$ storage capacity, long term cycle life, and superior kinetics.[10] Benefiting from the multiscale pores and heteroatom-containing functional groups, the as-obtained nanocomposite material exhibits a very high reversible capacity (1500 $mA\,h^{-1}\,g^{-1}$, i.e., much higher than commercial graphite) in its first lithiation/delithiation cycle, which is accompanied by a similar irreversible capacity.

Owing to its low cost, ready availability, and eco-friendliness, $TiO_2$, which exists in several polymorphic modifications (such as rutile, anatase, brookite, and bronze-$TiO_2$-B), is an attractive candidate for LIB anode materials. $TiO_2$-B has a high theoretical capacity of about 335 $mA\,h^{-1}\,g^{-1}$ and its pseudocapacitive mechanism of Li-storage as well as open channel structure makes it an ideal material for LIB application.[11] However, the sluggish electrode kinetics and mass transport require the downsizing of the $TiO_2$-B particles, but no scalable synthesis was available for real applications, so far. The classical synthesis of $TiO_2$-B, based on ion-exchange and calcination of layered titanates or on autoclave hydrolysis methods, is either difficult to scale up or takes long time. ILs have been successfully exploited in the synthesis of $TiO_2$ and other functional metal oxide nanoparticles, avoiding high-temperature and energy-intensive synthesis techniques.[12] The groups of Chen,[11] Mansfeldova,[13] Li,[14] and Wessel[15] recently revealed the creative use of ionic liquids for the fabrication of $TiO_2$-B, carbon nanotubes coated with $TiO_2$-B nanosheets (CNTs@$TiO_2$-B NSs), $TiO_2$ nanotube arrays, and $TiO_2$-B@anatase, respectively. The sol–gel synthesis of $TiO_2$ (anatase) and $TiO_2$-B, in the presence of various imidazolium-based ionic liquids with tetrafluoroborate and chloride counterions such as $[C_{16}mim][Cl]$, $[C_8mim][Cl]$, $[C_4mim][BF_4]$, and $[C_8mim][BF_4]$, was found to selectively engineer the final product in terms of the composition of the anatase/$TiO_2$-B phases.[13] The fractions of $TiO_2$-B and anatase in the product, as determined by integrating the voltammetric charge of the area corresponding to anatase or $TiO_2$-B peaks, was found to vary with the nature of the IL. The examination of the influence of the particular IL in obtaining the desired product revealed the key role of $[C_{16}mim][Cl]$ as surfactant. The highest amount of $TiO_2$-B obtained in the final product was for the sample prepared by combining $[C_4mim][BF_4]$ and $[C_{16}mim][Cl]$, whereas it remained low for other IL combinations. Interestingly, the $TiO_2$-B obtained by the IL-assisted synthesis method did not show the fibrous morphology, which is characteristic for the products obtained by solid-state synthesis.[16] Chen et al.[11] fabricated CNTS@$TiO_2$-B using $[C_4mim][BF_4]$ as a template for the in situ growth of $TiO_2$-B nanosheet arrays on CNTs through cation–$\pi$ interactions. An investigation of the influence of the amount of IL on the morphology of the hybrid material showed that $TiO_2$-B nanosheets tend to assemble on CNTs. This is not the case in the absence of ILs, where it was instead found to simply precipitate in the solution bulk. The high specific surface area, porous nature, and multiple electron/lithium pathways of the nanoarchitectured hybrid material combined with the pseudocapacitive behavior and reduced ion-diffusion path of the $TiO_2$-B nanosheets, attribute a high reversible capacity and superior rate capability, making it appropriate as electrode material. Li et al.[14] synthesized $TiO_2$ nanotube arrays from $Ti^0$ in 98 % wt % $[C_4mim][BF_4]$ in the presence of 2 % $H_2O$ as anodizing electrolyte. Unlike $TiO_2$ nanotubes obtained by the conventional ethylene glycol/$NH_3$ solution method, which get disintegrated during cycling, the IL-produced $TiO_2$ nanotubes (ILNTs) demonstrated excellent capacity retention without any microstructural defects for almost 1200 charge/discharge cycles.

The search for alternatives to carbonaceous anodes in large-scale electrochemical energy storage and power-oriented applications, has focused on Li alloying compounds ($Li_xM$, M = Sn, Si, Ge, Al, etc.) and conversion materials (e.g., CoO, $Co_3O_4$, $Mn_3O_4$, CuO, NiO), which promise extremely high capacities. As an example, the alloying reaction between

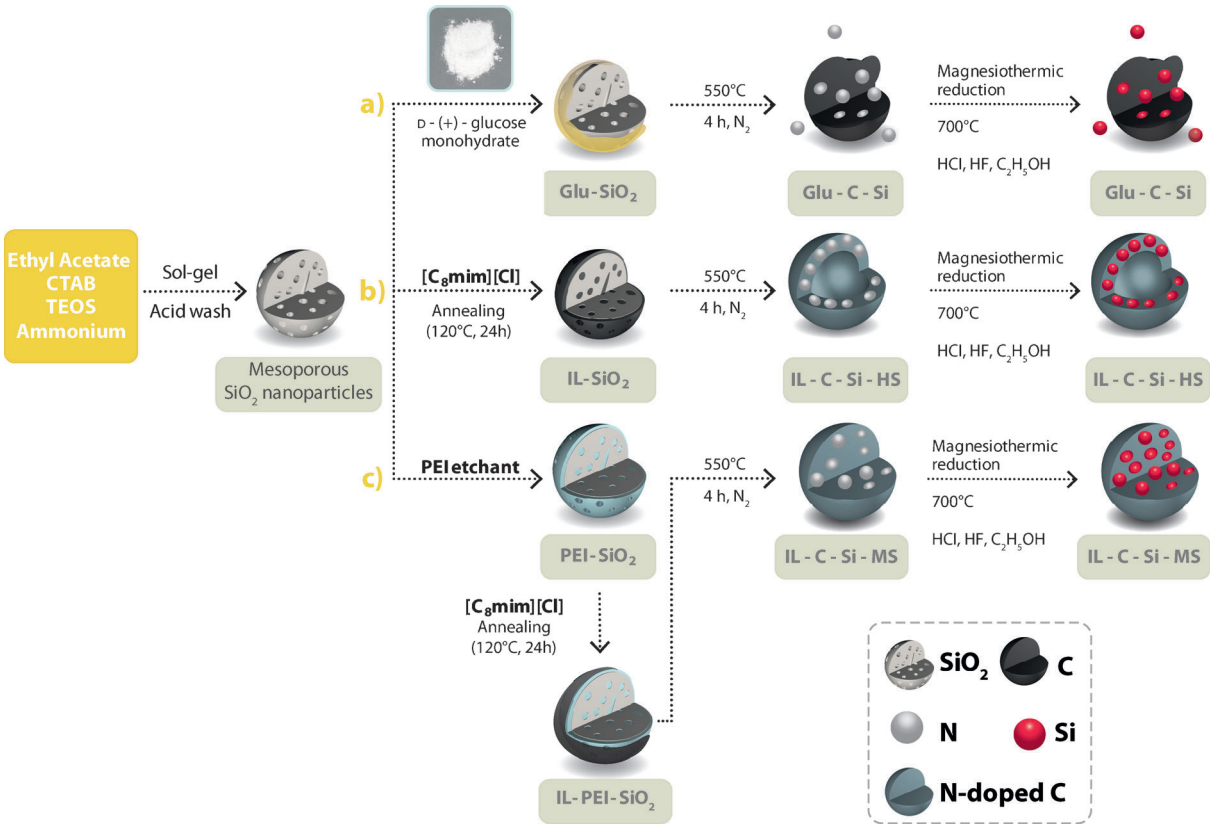


***Figure 3.*** Schematic illustration of the synthesis of different C/Si composites. a) Synthesis of glucose (Glu)-derived C/Si nanocomposite (Glu-C-Si) using Glu as carbon precursor; b) synthesis of IL-derived hollow spherical C/Si nanocomposites (IL-C-Si-HS), using IL as carbon and nitrogen precursor; and c) synthesis of mesoporous C/Si nanocomposites (IL-C-Si-MS), using PEI-$SiO_2$ as Si precursor.

Si or Sn and Li leads to $Li_{22}Si_5$ and $Li_{22}Sn_5$ with a corresponding theoretical capacity of 4200 $mA\,h^{-1}\,g^{-1}$ and 990 $mA\,h^{-1}\,g^{-1}$, respectively, whereas graphite has a theoretical capacity of 372 $mA\,h^{-1}\,g^{-1}$ ($LiC_6$).[17] However, their practical utilization in rechargeable LIBs is severely hampered by their huge volume expansion, up to 300% for Si during lithium-ion alloying/de-alloying, leading to swift capacity fading and large irreversible capacity. Many efforts have been made to solve this challenge, but the main approach consisted of downsizing the alloying material to the nanoscale to relieve internal stresses and is used to decrease the diffusion lengths of electrons and $Li^+$ ions.[17] However, reducing the size of particles to the nanoscale may lead to more safety hazard concerns, significant side reactions with the electrolyte, and difficulty in maintaining interparticle contacts. Moreover, the electrode tap density is decreased and thereby the available volumetric energy density. However, Ma and co-workers[18] recently reported a scalable method of encapsulating silicon (Si) nanocrystallites in a mesoporous N-doped carbon matrix in [$C_8$mim][Cl].[18] Through the careful selection of the IL carbon precursor, the pore size engineering of $SiO_2$, and by the help of surface-protected etching using polyethyleneimine (PEI), a nanocomposite (IL-C-Si-MS) with a uniform distribution of Si nanocrystals was obtained. The tight integration between Si and carbon provided the composite material with a good balance of mixed-conducting (ionic/electronic) properties and effective matrix, cushioning the Si volume change during cycling. In comparison to glucose-derived carbon, the IL-derived carbon resulted in a more uniform carbon coating and complete encapsulation of the $SiO_2$ nanoparticles, which could be explained as due to electrostatic interaction between the negatively charged $SiO_2$ (from the partial ionization of the silanol groups into $SiO^-$) and the IL cations, $[C_8mim]^+$ (Figure 3). Galvanostatic measurements displayed an impressive electrochemical performance of 1380 $mA\,h^{-1}\,g^{-1}$ reversible capacity at 200 $mA\,g^{-1}$, and excellent cyclability and rate performance up to 4 $A\,g^{-1}$. These were attributed to the synergic effect of the ultrafine Si nanocrystals and the mesoporous N-doped carbon matrix. Among tin-based Li-storage compounds, tin oxide ($SnO_2$) has been reported as the most promising anode candidate. $SnO_2$ is first irreversibly converted to tin ($Sn^0$) according to Equation (1). Subsequently, the in situ Sn phase formed could store and release up to 4.4 Li per Sn, according to the Li–Sn alloying/de-alloying reactions as shown in Equation (2).

$$SnO_2 + 4\,Li^+ + 4\,e^- \rightarrow Sn + 2\,Li_2O \quad (1)$$

$$Sn + x\,Li^+ + x\,e^- \rightarrow Li_xSn\ (0 \le x \le 4.4) \quad (2)$$

However, like other alloying materials, its practical application is greatly limited by the huge volume change during charge/discharge. Once again, ionic liquids demon-

  

strated their highly beneficial effect in the preparation of a $SnO_2$/graphene composite electrode with improved electrochemical performances. $SnO_2$ nanoparticles monodispersed on the surface of reduced graphene oxide have been developed by an ultrasonic-assisted oxidation–reduction reaction between $Sn^{2+}$ and graphene oxide in a choline chloride/ethylene glycol based pseudo-IL under ambient conditions.[19] Choline chloride forms a strong hydrogen bond with ethylene glycol through its chloride function, resulting in a homogeneous liquid with a significant decrease in the melting point with respect to the individual solvents. As anode material for LIBs, $SnO_2$/graphene nanocomposite showed satisfactory cycling stability of 535 $mA\,h^{-1}\,g^{-1}$ at 100 $mA\,g^{-1}$ after 50 cycles, which is significantly higher as compared to bare $SnO_2$ nanocrystals. The improvement in cycling stability of $SnO_2$/graphene composite over bare $SnO_2$ nanoparticles is to be credited to the buffering effect of graphene sheets, which alleviates the volume expansion/crushing of Sn nanocrystals during alloying/de-alloying.

In recent years, three-dimensionally ordered macroporous (3DOM) films in the form of inverse opals have attracted much attention as electroactive materials owing to a number of benefits such as bicontinuous networks, large accessible areas, short diffusion lengths, and fast transportation of the electrolyte inside the porous structure, resulting in an improvement of both the rate capability and cycling behavior of the electrode materials. For the fabrication of 3DOM germanium films, chemical vapor deposition (CVD) onto silica colloidal crystal templates has been widely investigated, because the resulting films display interesting battery performances. Unfortunately, due to the reaction between Ge and the $SiO_2$ template when the CVD is performed above 300 °C, inactive $Li_2O$ and hollow Ge, instead of inverse opal structure were inevitably formed. Moreover, the electrodeposition of Ge in aqueous organic solvents (e.g., poly(ethylene glycol)) and conventional molten salts has been prohibited by hydrogen evolution, low current efficiency, and high energy cost. Recently, Endres et al.[20] reported the direct electrodeposition of 3DOM Ge at room temperature from ILs.[21] This approach, performed in $[C_2mim][Tf_2N]$, had several advantages such as the use of polystyrene (PS) instead of silica templates, which avoids Ge oxidation and results in the production of highly ordered macroporous structures of nanocrystalline germanium leading to a high electrochemical performance. The IL-based 3DOM Ge film exhibited a first cycle reversible capacity of 1024 $mA\,h^{-1}\,g^{-1}$ and retained ca. 844 $mA\,h^{-1}\,g^{-1}$ after 50 cycles at 0.2 C. In contrast, nano-Ge films were reported to deliver only about 611 $mA\,h^{-1}\,g^{-1}$ for the same number of cycles. The 3DOM film obtained by IL-assisted deposition offers a number of advantages such as providing enough free volume to buffer the germanium's expansion–contraction volume stress and offering multiple pathways for electrons and ions. Moreover, the available free volume mitigates the crack formation that could be triggered due to the continuous solid electrolyte interface (SEI) layer growth during cycling.

The capacity limitations of present LIB electrodes can be avoided using active materials capable of reversibly incorporating more than one Li per 3*d* metal. Metal oxides, fluorides, oxyfluorides, sulfides, nitrides, and phosphides have been shown to exhibit large lithium capacities through conversion processes leading to the formation of the metal and $Li_2O$. However, these processes commonly show a marked hysteresis in voltage between charge and discharge, imparting limitation on both energy efficiency and power capabilities.

$Fe_2O_3$ is one of the most ideal materials because of its high specific capacity (theoretically 1007 $mA\,h^{-1}\,g^{-1}$), natural abundance, low cost, and benignity. The awkward and additional complexity of traditional synthesis routes used to fabricate conversion-type materials, including the need to select the appropriate solvent and calcination temperature, the necessity to completely remove shape-controlling ions, and their time-consuming and energy-intensive demanding nature, has been an impetus toward hunting for more facile and environmentally friendly synthesis routes. In this regard, IL and IL-assisted methods have proven to be champion in reducing the aforementioned difficulties. The groups of Lian,[22] Xu,[23] Ma,[24] and Coa[25] efficaciously synthesized shape-controllable $Fe_2O_3$ using $[C_4mim][Cl]$, $[C_8mim][(FeCl_4)]$, $[C_3mim][I]$, and $[C_4mim][BF_4]$, respectively. Hematite of various engineered morphologies such as nanoparticles, mesoporous hollow microspheres, and microcubes were successfully obtained by IL-assisted hydrothermal methods.[22] $[C_4mim][Cl]$ is found to have a significant influence on the morphology of the iron oxide, because it lowers the surface tension, resulting in a high nucleation rate and thereby the formation of very small particles. Moreover, increasing the amount of $[C_4mim][Cl]$ was reported to induce morphological changes, for instance, from monodispersed nanoparticles to superstructures (i.e., mesoporous hollow microspheres and microcubes) due to Ostwald ripening. The formation of unique, self-assembled nanostructures by the IL-assisted route was explained as a result of the extended hydrogen bond-co-π–π stacking mechanism. Despite its scientific and technological importance, the low electrical conductivity, high vulnerability to agglomeration, and poor cycle life due to the large volume change upon charge/discharge have hindered the practical application of $Fe_2O_3$ in its bulk form.

As part of the effort to overcome these challenges, Balach et al.[26] recently prepared $Fe_2O_3$ nanoparticles confined in porous, N-doped, hollow carbon spheres (NHCSs) prepared by grafting a thin layer of poly(ionic liquid) (PIL) as carbon and nitrogen source. When utilized as anode material for LIBs, the as-synthesized $Fe_2O_3$–NHCSs nanocomposite exhibited a high reversible capacity of 1120 $mA\,h^{-1}\,g^{-1}$ at the rate of 100 $mA\,g^{-1}$, with a coulombic efficiency of 98% at a rate of 500 $mA\,g^{-1}$ after 65 cycles. The improved performance was attributed to the ability of the 3D thin carbon layer, which builds up fast electron transport channels while serving as a physical buffering layer for the volume change of $Fe_2O_3$ nanoparticles during charge/discharge. In another work, Park et al.[27] reported the in situ and direct deposition of $Fe_2O_3$ nanoparticles on $[C_4mim][BF_4]$-functionalized carbon nanotubes (Figure 4). The binder-free, self-standing film of IL-CNT/$Fe_2O_3$ demonstrated up to 413 $mA\,h^{-1}\,g^{-1}$ discharge capacity, with coulombic efficiency and capacity retention of 98% and 67%, respectively, after 50 charge/

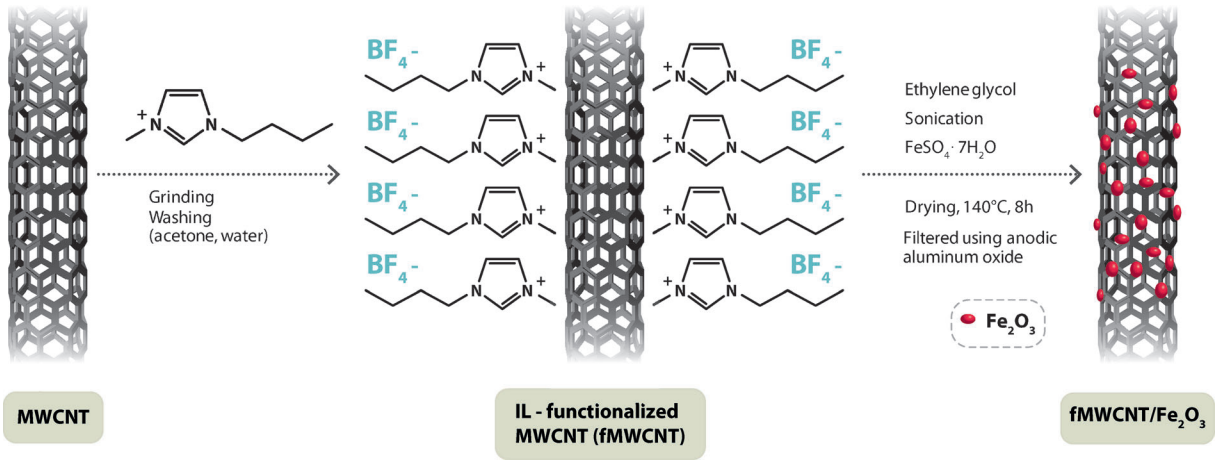


***Figure 4.*** Representation of the synthesis of IL-functionalized multiwall carbon nanotubes/$Fe_2O_3$ nanocomposite material.

discharge cycles. The IL acted as the CNT dispersant, improving the production of the latter and providing a favorable interfacial contact between CNT and $Fe_2O_3$. In addition to the aforementioned electroactive materials, the synthesis of Ni–P alloys,[28,29] Si thin films,[30] $MoO_2$ nanosheets,[31] Sb-doped $SnO_2$,[32] mesoporous rutile $TiO_2$,[33] IL-derived N-doped carbon-coated $Li_4Ti_7O_{12}$, $M_2S_3$ (M = Bi, Sb),[34] and several other anode materials have been reported using ILs.

In general, innovative IL-assisted synthesis methods open a multitude of possibilities for the development of various anode materials for LIBs, rekindling the motive toward designing best performing electrode materials.

*Cathode materials*

Inspired by the seminal work of Recham et al., [35–37] considerable attention has recently been paid to the ionothermal method as a novel and green synthesis route to fabricate cathode materials with engineered properties. Tarascon and co-workers embarked a proof of concept experiment utilizing iron oxalate ($FeC_2O_4{\cdot}2H_2O$) and $LiH_2PO_4$ as iron-, lithium-, and phosphate-precursors, and $[C_2mim][Tf_2N]$ as a reaction medium. The single-phase $LiFePO_4$ obtained by heating the suspension at lower temperature (as low as 250 °C) exhibited satisfactory electrochemical performance. In light of such positive results, extensive studies of several ILs as reaction media for the synthesis of a variety of electroactive cathode materials has been demonstrated.[37,38] Ionic liquids used in the first proof-of-principle experiments evidenced to have a strong impact on the $LiFePO_4$ nucleation/growth rate, while at the same time behaving as a structural directing agent. Varieties of ILs were scrutinized with respect to the variation of the anionic components [e.g., $BF_4^-$, $Tf_2N^-$, $CF_3SO_3^-$, $C(CN)_3^-$, and $Cl^-$], cationic centers (pyrrolidinium, imidazolium, and pyridinium), and their carbon chain lengths (C2–C8) linked to the imidazolium cations, with special emphasis on the resulting physicochemical characteristics of the ILs.

For instance, needle-shaped (along the [010] direction) particles of $LiFePO_4$ were obtained by modifying the polarity of the medium, the $[C_2mim]^+$ cation, with appended polar nitrile groups. On the other hand, platelet-like particles (along the [020] direction) were evidenced in the presence of less polar ILs with longer aliphatic chains (i.e., $[C_{18}mim]^+$ cation). The two different morphologies were explained in terms of competing surface energies, which in turn are linked to the nature of the IL, its solvating strength, polarity, and propensity to specifically adsorb on one surface. Thus, the IL-induced polarity of the reacting medium and its solvating properties influence the surface energy minimization of the system, thereby affecting the crystal growth. The obtained $LiFePO_4$ proved to be electrochemically active, resulting in a specific capacity of 150 $mA\,h^{-1}\,g^{-1}$ at 15 $mA\,g^{-1}$ without any carbon coating. Further investigations proved that the ionothermal synthesis can be extended to other well-known inorganic cathode materials beyond $LiFePO_4$ by simply changing the nature of the 3d-metal precursor, while keeping the same IL and experimental conditions as illustrated in Table 2. In this regard, the method was successfully applied to the synthesis of cathode materials derived from the olivine-type ($LiMPO_4$, M = Mn, Co, and Ni)[37,39] and other electrode materials comprising of: 1) $(SiO_4)^{4-}$ instead of $(PO_4)^{3-}$ (e.g., $Li_2MnSiO_4$, $Li_2FeSiO_4$),[40,41] 2) incorporating $F^-$ in $SO_4^{2-}$ (e.g., $LiFeSO_4F$, $LiMnSO_4F$),[42] and 3) in $PO_4^{3-}$ as mixed anionic lattice (e.g., $LiFePO_4F$, $LiTiPO_4F$),[43–45] 4) conversion cathode materials (e.g., $FeF_3$),[46–49] 5) other battery chemistries, for example, using $Na^+$ rather than $Li^+$ as guest ions (e.g., $NaMPO_4F$, M = Fe, Mn, $Fe_{1-x}Mn_x$),[35,50] and 6) oxides, such as $LiNi_{0.5}Mn_{1.5}O_4$.[51]

Stimulated by the aforementioned findings, Chen et al.[52],[53] successfully synthesized $LiFePO_4$ by an electrochemically-assisted method using $[C_2mim][Tf_2N]$ as electrolyte bath, containing $FeCl_2$ and $Li_3PO_4$ at 275 °C. The $LiFePO_4$ formation takes place through two steps as evidenced by the presence of two redox peaks at $E = -0.1$ V vs. $Ag^+/Ag^0$ [Eq. (3)] and $E = 0.1$ V vs. $Ag^+/Ag^0$ [Eq. (4)], resulting in the overall reaction represented in Equation (5). Moreover, high performance $LiFePO_4$ nanorod-structured material was successfully synthesized making use of the synergetic effect of ILs and surfactant molecules.[53]

  

***Table 2:*** List of cathode materials synthesized in ILs, enlisting the nature of the precursors, the ILs used, and the experimental conditions. TEOS = tetraethyl orthosilicate.

| Cathode materials | Precursor | ILs | $T_{reaction}$ [°C] | Particle size | Ref. |
|---|---|---|---|---|---|
| $LiFePO_4$ | $LiH_2PO_4$, $FeC_2O_4{\cdot}2H_2O$ | $[C_2mim][Tf_2N]$ | 250 | 150–300 nm | [35] |
| | $Li_3PO_4$, $FeCl_2$ | $[C_2mim][Tf_2N]$ | 275 | 500 nm | [52] |
| | $FeSO_4{\cdot}7H_2O$, LiOH, $H_3PO_4$ | $[C_4mim][BF_4]$ | 240 | 200 nm | [53] |
| $LiMnPO_4$ | $LiH_2PO_4$, $MnC_2O_4{\cdot}2H_2O$ | $[C_2mim][Tf_2N]$ | 250 | 100–400 nm | [39, 54] |
| $LiMPO_4$ (M = Ni, Co) | $LiH_2PO_4$, $MC_2O_4{\cdot}2H_2O$ | $[C_2mim][Tf_2N]$ | 250 | 800–1000 nm | [37–39] |
| $LiFePO_4F$ | $Li_3PO_4$, $FeF_3$ | triflate | 260 | < 50 nm | [43–45] |
| $LiTiPO_4F$ | $Li_3PO_4$, $TiF_3$ | $C_2$-OH | 260 | < 50 nm | [43–45] |
| $LiFeSO_4F$ | $FeSO_4{\cdot}H_2O$, LiF | $[C_2mim][Tf_2N]$ | 280 | 600–1200 nm | [42] |
| $LiMnSO_4F$ | $MnSO_4{\cdot}H_2O$, LiF | $[C_2mim][Tf_2N]$ | 280 | 600–1200 nm | [42] |
| $FeF_3$ | $Fe(NO_3)_3{\cdot}9H_2O$, $[C_4mim][BF_4]$ | $[C_4mim][BF_4]$ | < 50 | 10 nm | [46] |
| | $FeF_3{\cdot}3H_2O$ | $[C_4mim][BF_4]$ | 250 | 10 nm | [49] |
| $FeF_3$/graphene hybrid | $Fe(NO_3)_3{\cdot}9H_2O$, natural flakes graphite, $[C_4mim][BF_4]$ | $[C_4mim][BF_4]$ | 80 | – | [48] |
| nanowired $FeF_3$ | $Fe(NO_3)_3{\cdot}9H_2O$, SWCNTs,[a] $[C_4mim][BF_4]$ | $[C_4mim][BF_4]$ | 80 | 10 nm | [47] |
| $Li_3V_2(PO_4)_3$ | $LiOH{\cdot}H_2O$, $V_2O_5$, $H_3PO_4$ | $[C_2mim][BF_4]$, $[C_2mim][OTf]$, $[C_2mim][OAc]$ | 200 | 0.2–1 μm | [59] |
| | $V_2O_5$, $H_2C_2O_4{\cdot}NH_4H_2PO_4$, $Li_2CO_3$ | $[PYR_{14}][Tf_2N]$, $[C_2mim][Tf_2N]$ | – | 50 nm | [58] |
| $Li_2MnSiO_4$ | $Mn(CH_3OO)_2{\cdot}2H_2O$, $LiCH_3COO_2{\cdot}H_2O$, TEOS | $[C_2mim][BF_4]$, $[C_4mim][BF_4]$ | – | 50–80 nm | [40] |
| $LiNi_{0.5}Mn_{1.5}O_4$ | $Mn(CH_3COO)_2{\cdot}4H_2O$, $Ni(CH_3COO)_2{\cdot}4H_2O$ | $[C_{12}mim][Br]$ | – | 700 nm | [51] |

[a] SWCNT = single-walled carbon nanotube.

$$Fe^{III} + e^- \rightarrow Fe^{II} \quad (E \approx -0.1\ V \text{ versus } Ag^+/Ag^0) \tag{3}$$

$$Fe^{II} \rightarrow Fe^{III} + e^- \quad (E \approx 0.1\ V \text{ versus } Ag^+/Ag^0) \tag{4}$$

$$Fe^{III} + Li_3PO_4(s) + e^- \rightarrow LiFePO_4(s) + 2\,Li^+ \tag{5}$$

Extending the success stories of LFP synthesis by the ionothermal route, Barpanda et al.[54] synthesized $LiMnPO_4$ utilizing a variety of ILs as reaction media in the temperature range of 220–250 °C at ambient pressure. The size and shape of $LiMnPO_4$ could be tuned by carefully varying the nature of the IL medium. For instance, the attachment of OH groups to a $[C_2mim][Tf_2N]$ significantly improved the precursor solubility, lowering the reaction temperature from 250 °C to 220 °C and leading to the formation of 200–400 nm $LiMnPO_4$ particles. Conversely, replacing the $Tf_2N^-$ anion with the smaller and more thermally stable triflate anion ($CF_3SO_3^-$) resulted in much easier grain growth, forming slightly larger (300–700 nm) particles. Moreover, lengthening the alkyl chain increases the microphase separation (chain/ring), thereby triggering faster reaction kinetics, which ultimately results in an increase of the particle size from 3–4 μm (for $C_6$–$C_{10}$) to 50 μm (for $C_{18}$). After successful carbon coating, the IL-synthesized $LiMnPO_4$ had a discharge capacity close to 100 $mA\,h^{-1}\,g^{-1}$ (at C/20) at a potential of 4.1 V, with excellent cycling reversibility.

Increasing the operating cell voltage of the cathode material is one way to improve the energy density of today's LIBs and this could be achieved by simply combining the inductive effect of the $(PO_4)^{3-}$ group and the high electronegativity of the $F^-$ anion by forming fluorophosphates. Recently, it has been reported that electroactive $LiFeSO_4F$ could be crystallized from $[C_2mim][Tf_2N]$ in a tavorite phase.[45] This material possesses 3D channels that, favoring $Li^+$ ion migration, lead to higher electronic and ionic conductivities and slightly higher voltage compared with $LiFePO_4$. Because of its lower decomposition temperature (~375 °C) and instability in water, $LiFeSO_4F$ could never be synthesized, neither by a ceramic process nor in aqueous medium. [55]

The electrochemical performance of the as-prepared $LiFeSO_4F$ material was found to be very appealing: over 140 $mA\,h^{-1}\,g^{-1}$ reversible specific capacity (very close to the theoretical capacity of 151 $mA\,h\,g^{-1;}$ $Fe^{2+/3+}$ redox potential at 3.6 V) at a rate of 15 $mA\,g^{-1}$ without either particle downsizing or carbon coating. Besides, the higher ionic conductivity of $LiFeSO_4F$ (~$4\times10^{-6}$ $S\,cm^{-1}$), compared to $LiFePO_4$ (~$2\times10^{-9}$ $S\,cm^{-1}$) suggests a much higher lithium diffusion coefficient in $LiFeSO_4F$, explaining why high rate capabilities for Li-insertion/extraction in $LiFeSO_4F$ are achievable without the need to go for nanosized particles as for $LiFePO_4$. Following the same experimental protocol as used for the synthesis of $LiFeSO_4F$, the production of electrochemically active, triplite-type $LiFe_{1-x}M_xSO_4F$ (M = Mn, Ni, Co) in $[C_2mim][Tf_2N]$ was achieved.[44,55] The extensive edge-sharing chains of $MO_4F_2$ octahedra in the triplite structure raises the

  

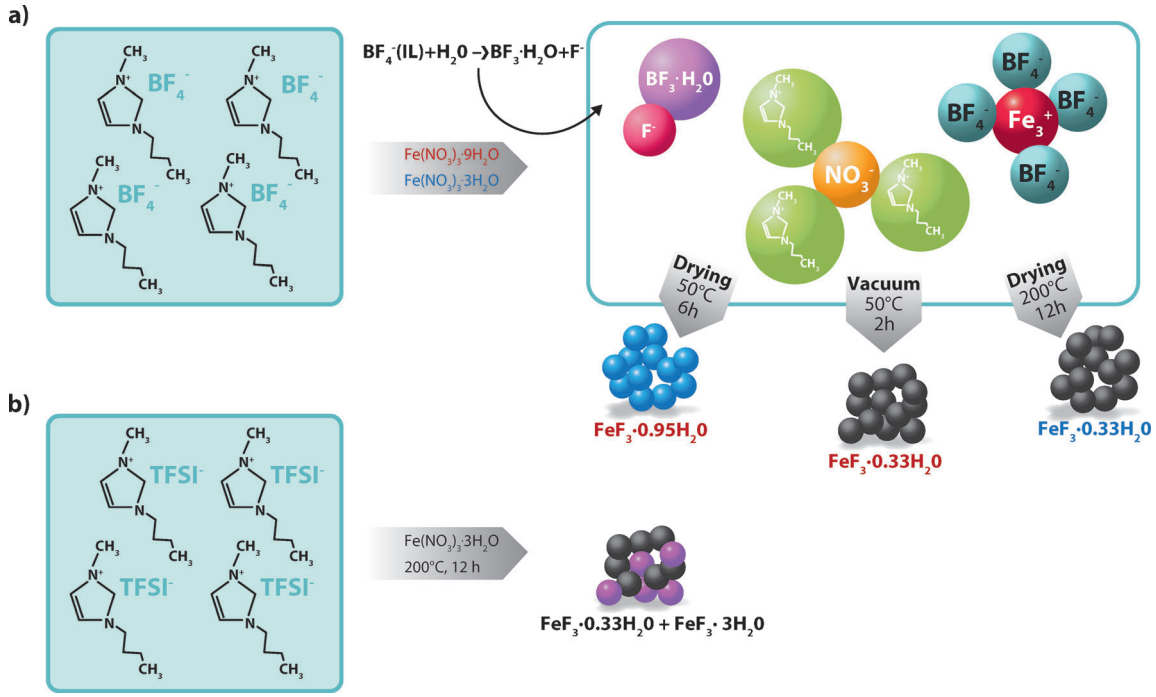


***Figure 5.*** Synthesis of hydrated iron-based fluoride, a) from $[C_4mim][BF_4]$ ionic liquid and $Fe(NO_3)\cdot 9\,H_2O$ or $Fe(NO_3)_3\cdot 3\,H_2O$ precursors and b) from $[C_4mim][TFSI]$ ionic liquid and $Fe(NO_3)_3\cdot 3\,H_2O$ precursors. TFSI = $(CF_3SO_2)_2N$.

$Fe^{2+}/Fe^{3+}$ redox couple to 3.9 V vs. Li, which is ca. 0.3 V higher than that of tavorite (corner-shared chains), making it a high-energy-density cathode material. Besides the higher $Fe^{2+}/Fe^{3+}$-redox-couple gain, exceeding $LiFePO_4$ by ca. 0.45 V, the newly discovered triplite-phase cathode material is capable of providing a capacity of about 125 $mA\,h^{-1}\,g^{-1}$ with a much lower volume change (~0.6%) during Li (de)insertion than $LiFePO_4$ (~7%) and $LiFePO_4F$ (~10%). Unfortunately, the $Li^+$ diffusion in the indistinguishable Fe/Li sites is relatively slow, limiting the power availability.

In the search for high capacity cathode materials, $FeF_3$ has attracted sizeable interest as the next-generation electroactive material because of its high specific capacity, exceeding 237 $mA\,h^{-1}\,g^{-1}$ [1 $e^-$ transfer, Eq. (6)], which is significantly higher than that of $LiFePO_4$ (170 $mA\,h^{-1}\,g^{-1}$).[46,49] An even higher theoretical capacity of 712 $mA\,h^{-1}\,g^{-1}$ could be provided by the conversion reaction, in which $FeF_3$ is reduced to an Fe and LiF composite [Eq. (7)].

$$FeF_3 + Li^+ + e^- \rightarrow LiFeF_3 \quad (6)$$

$$LiFeF_3 + 2\,Li^+ + 2\,e^- \rightarrow 3\,LiF + Fe \quad (7)$$

Inspired by the successful carbon-free fabrication of a high-performance $LiFePO_4F$, Li *et al.* [46] synthesized nanostructured iron-based fluoride ($FeF_3$), using $[C_4mim][BF_4]$ as a reaction medium and fluorine source and iron(III)nitrate nonahydrate ($Fe(NO_3)_3\cdot 9\,H_2O$) as iron precursor (Figure 5). Compared to the mechanical ball milling and aqueous chemical approaches, the IL-assisted synthesis of $FeF_3$ exhibits several advantages such as:

1) The obtainment of well-defined nanostructures of high crystallinity at about 50 °C, i.e., close to room temperature.
2) The possibility of applying vacuum treatments to achieve desired microstructures, morphologies, and crystallization degrees.
3) The availability of an eco-friendly and operationally safer fluoride ion source.
4) The possibility of affecting particle growth and agglomeration, resulting in the formation of monodisperse nanocrystals.
5) Ensuring better reproducibility as a result of fewer reagents and more controlled reaction environments.

The chemical environment, temperature, and nature of the IL play crucial roles as far as the final product quality is concerned.[49] One of the steps in the preparation of $FeF_3$ involves the release of $F^-$ ions through hydrolysis of the IL anion ($BF_4^-$) and the structure-directing effect of the IL. Use of a hydrophobic $Tf_2N^-$, instead of the hydrophilic $BF_4^-$, results in an incomplete transformation as indicated by the coexistence of the target product ($FeF_3\cdot 0.33\,H_2O$) and unreacted $FeF_3\cdot 3\,H_2O$ compound (Figure 5).

High-performance CNT-wired iron fluoride [47] has been made using $[C_4mim][BF_4]$, which acts as precursor, dispersant, and binder. Analogously, iron fluoride/graphene sheet hybrid nanostructures [48] were successfully obtained with the same IL.

Among the highly promising $Li_3M_2(PO_4)_3$ (M = Ti, Fe, V) cathode materials with a NASICON structure, $Li_3V_2(PO_4)_3$ (LVP) is of particular interest because it can theoretically exchange three $Li^+$ ions per formula unit within the potential

  

range of 3.0 V to 4.3 V vs. $Li^+/Li$, resulting in a maximum discharge capacity of 197 $mA\,h^{-1}\,g^{-1}$.[56-58] However, monoclinic $Li_3V_2(PO_4)_3$ displays a low intrinsic electronic conductivity (i.e., $2.4\times10^{-7}\,S\,cm^{-1}$) at room temperature, excluding its use in applications in which rate capability is the prerequisite. Amongst the various synthesis and processing approaches that have been recently employed to fabricate LVP, the ionothermal synthesis in IL media has proven new opportunities to fully exploit the material's intrinsic potential. Li et al.[57] recently synthesized a high performance, nanostructured $Li_3V_2(PO_4)_3$ using $[C_2mim][OTf]$, $[C_2mim][BF_4]$, and $[C_2mim][OAc]$ as reaction media as well as structure-directing agents. The size and shape of particles were highly dependent on the nature of the IL applied. While 0.2 μm particles with irregular shape were obtained for the material synthesized in $[C_2mim][BF_4]$, relatively smaller particles with uniform size distribution were achieved for the material fabricated in $[C_2mim][OAc]$. The differences in the particle sizes were explained to be due to the variations in the surface tension; the larger the surface tension of the selected IL is, the higher is the surface free energy and therefore the size of the obtained crystals.

In the 3.0–4.3 V voltage range, the $Li_3V_2(PO_4)_3$/C composite material prepared in $[C_2mim][OTf]$) delivered discharge capacities of 131.7 $mA\,h^{-1}\,g^{-1}$ and 113.7 $mA\,h\,g^{-1}$ at charge/discharge rates of 3.94 $mA\,g^{-1}$ and 19.7 $A\,g^{-1}$, respectively, after 50 cycles. The noteworthy electrochemical performance is attributed to the formation of ultrafine and uniform $Li_3V_2(PO_4)_3$ with the least agglomeration and an enhanced ion diffusion and electron conductivity. Very recently, Balducci et al.[58] reported an IL-assisted synthesis of nanostructured, carbon-coated $Li_3V_2(PO_4)_3$ particles through the careful selection of highly viscous and thermally stable ILs, $[C_4C_1pyr][Tf_2N]$ and $[C_2mim][Tf_2N]$, which serve both as solvent and carbon precursors during the sol-gel synthesis. The nanosized structure of the material shortens the diffusion paths, while maximizing the contact area between the active material and the electrolyte, leading to an enhanced $Li^+$ diffusion. At current rates as high as 7.88 $A\,g^{-1}$, the fabricated $Li_3V_2(PO_4)_3/[C_4C_1pyr][Tf_2N]$ electrode material delivered a reversible capacity of nearly 100 $mA\,h^{-1}\,g^{-1}$, whereas maintaining 99% of the initial capacity even after 100 cycles at rates higher than 10 $A\,g^{-1}$. This shows the aptness of the IL-assisted sol–gel synthesis method to obtain such excellent power capability and cycling performance, whilst at the same time substantiating the suitability of $Li_3V_2(PO_4)_3$ as high-power cathode material.

One of the approaches to increase the capacity of cathode materials derives from the development of materials that could afford more than one electron reversible exchange per transition metal. Orthosilicates ($Li_2MSiO_4$, M = Fe, Mn, Co, Ni) could be ideal frameworks for the reason that the $(SiO_4)^{4-}$ group would theoretically allow the 3d-transition metal to change its valence between +2 and +4, resulting in two lithium de/-intercalation per formula unit. Amid the orthosilicate family compounds, $Li_2MnSiO_4$ is more attractive, for instance, as compared to $Li_2FeSiO_4$, because the highest oxidation state of Mn (+4) is more accessible than in Fe. Allowing the extraction/insertion of two $Li^+$ ions, $Li_2MnSiO_4$ possesses a theoretical capacity of 333 $mA\,h^{-1}\,g^{-1}$ based on the $Mn^{2+}/Mn^{3+}/Mn^{4+}$ redox couple.[50] However, although noticeable progress has been made with a number of methods aiming at circumventing the low conductivity and structural instability of the fully lithium-depleted material ($Li_0MnSiO_4$) its performance is still insufficient for practical battery applications. Recently, ionothermal synthesis has enabled the formation of uniformly dispersed $Li_2MnSiO_4$ using $[C_2mim][BF_4]$ and $[C_4mimBF_4]$ as reaction media, with the latter IL imparting better performance to the resulting cathode material.[40] The $Li_2MnSiO_4$/C composite cathode material made from $[C_4mim][BF_4]$ presents smaller particle size and more favorable electrochemical properties, such as high-rate capability and cycling stability with a maximum discharge capacity of 218.2 $mA\,h^{-1}\,g^{-1}$ and a reversible capacity of 175.7 $mA\,h^{-1}\,g^{-1}$ in the 50th cycle, than the product obtained from $[C_2mim][BF_4]$. These observed differences could be explained to be due to the higher viscosity and lower surface tension of $[C_4mim][BF_4]$, in which the presence of the longer alkyl chain of the cation leads to a faster nucleation process, resulting in smaller nanocrystals. The excellent performance of the resulting $Li_2MnSiO_4$/C is mainly attributed to the peculiar role of the IL resulting in a uniform dispersion of small $Li_2MnSiO_4$ particles combined with an extremely effective carbon coating, which promotes the overall electronic conductivity.

In general, IL-assisted ionothermal syntheses offer special features that could not be obtained from other high-boiling molecular solvents. Modifying the structure and polarity of ILs enables a better control of the final material properties such as particle size, shape, structure, and electrochemical performance. For instance, the low surface tension of ILs enables high nucleation rates, and, as a consequence, smaller particle sizes. ILs also serve as electronic and steric stabilizers, leading to the development of new materials, which could otherwise not be synthesized in molecular solvents due to their inherent instability. Moreover, ILs can act as "all-in-one" solvent-reactant-template in the synthesis of tailored inorganic materials, a peculiar characteristic which is not offered by other solvents.

#### 2.1.2. *Ceramic Electrolytes*

Bearing in mind the safety concerns of large format LIBs, replacing state-of-the-art organic liquid electrolytes with solid electrolytes would bring a new perspective, enabling high-energy Li-ion battery chemistry with an intrinsically safe cell design. However, though recently the search for good solid electrolytes constitutes a major goal, the few candidates which do exist today suffer primarily either from narrow electrochemical window or too low ionic conductivity, impending their real-time practical applications. Reinvigorated by the discovery of alkali metal fluorosulfates ($AMSO_4F$), noticeably the $NaMSO_4F$ phase obtained by isothermal synthesis, displaying a room temperature conductivity of $\sim10^{-7}\,S\,cm^{-1}$, Barpanda et al.[59] continued the exploration of other fluorosulfate-based solid electrolyte materials of higher intrinsic conductivity. Mindful of the versatility evidenced with the synthesis of a variety of

  

electrode materials, the IL-based synthesis route was used in an impetus to find further fluorosulfate members to develop new ceramic electrolyte materials that enable switching from thin-film to bulk technology in all solid-state batteries. $LiZnSO_4F$, a fluorosulfate material of $LiTiOPO_4$-type structure, obtained by using $[C_2mim][Tf_2N]$, showed a room temperature ionic conductivity ranging between $10^{-5}$ and $10^{-7}$ S cm$^{-1}$ on pressed pellet samples, four orders of magnitude higher than the IL-free $LiZnSO_4F$ ($10^{-11}$ S cm$^{-1}$) electrolyte. The new material also showed an electrochemical stability window extending from 0 to 5 V (vs. Li).[59] The increment in ionic conductivity was proposed due to the effect of encapsulation of the $LiZnSO_4F$ grains by a layer of IL that offers the proper percolation network for ionic conduction. However, the $\log(\sigma) = f(1/T)$ plot for $LiZnSO_4F$ was found to impeccably follow the Arrhenius law, raising questions about the role of the IL, whose contribution should obey the Vogel–Fulcher–Tammann (VTF) model. Thus, the increment in ionic conductivity of the $LiZnSO_4F$-IL sample could, most likely, be related to a Li-bearing IL layer grafted onto the surface of the $LiZnSO_4F$ particles. For a while, Barpanda and co-workers sustained their effort towards understanding the underlying mechanism of such increment in ionic conductivity for the IL-assisted synthesized $LiZnSO_4F$. The presence of a thin layer of IL attached to the $LiZnSO_4F$ surface resulted in the formation of a slightly Li-rich ceramic IL composite claimed to contribute to the improvement in conductivity.[60] With the intention of attesting the flexibility of the IL-grafting-induced conductivity enhancement and its crystal-structure-independent nature, this phenomenon was extended to other non-isostructural Li-metal fluorosulfate family members such as $LiMSO_4F$ (M = Co, Mn). Thus, the IL grafting can be utilized as an alternative process for the synthesis of ceramic–IL composites endowed with much higher ionic conductivity, very close to the benchmarking range needed for solid electrolyte applications. However, since the application of ionothermal syntheses for the fabrication of composite electrolytes is in its infant stage, extra efforts are needed to understand the governing mechanisms and to apply them to the synthesis of other materials such as conventional oxide- and polyanionic-based solid electrolytes.

#### 2.1.3. Current Collectors

Current collectors are considered as inactive components in the battery, thus only reducing the gravimetric and volumetric energy densities of the system, although they serve as electrical conductor and mechanical support, and dissipate heat from the cell. Conventional current collectors used in LIBs are composed of two-dimensional (2D) flat metal foils. However, the most promising way to obtain high energy density and power capability on a limited surface area is to integrate current collectors in a three-dimensional (3D) configuration.[61-65] Three-dimensional current collectors can potentially offer several advantages like the possibility of higher mass loading without delamination of electrode materials or enhanced penetration due to the high surface area.[66] In this regard, electrodeposition has been the method of choice to coat and/or modify conducting surfaces with complicated geometries, even at low temperatures. With electrodeposition, the morphologies of the electrode materials can be controlled. Thus this method is particularly suitable for the realization of nanoscale architectures. Although many different materials have been investigated as cathode current collectors, aluminum (Al) is considered to be the metal of choice as high voltage current collector (up to 4.5 V vs. $Li^+/Li$) in LIBs, due to its low price, ready availability as reasonably high-purity thin foils and plates, good electric conductivity in terms of volume and mass, and the aptitude to form a passive surface layer. However, with an electrode potential of + 1.3 V vs. $Li^+/Li$, Al cannot be deposited from aqueous media. The well-known SIGAL process, involving alkylaluminum compounds in aromatic solvents, is hazardous owing to the high flammability of the aluminum precursors used, and requires the strict exclusion of oxygen.[67,68] However, recently, Perre et al.[62] demonstrated the selective electrodeposition of free-standing aluminum nanostructured rods of controlled size by using nanoporous alumina template membranes. The process is based on the reduction of $Al_2Cl_7^-$ in an IL-based $[C_2mim][Cl]$:$AlCl_3$ (1:2 ratio) electrolyte bath.

Very recently, Poetz and co-workers[61] successfully fabricated a 3D current collector, based on a nonwoven polymer, plated with a thin Ni-layer by chemical reduction and subsequent electrodeposition of an aluminum layer from $[C_2mim][Cl]$ mixed with $AlCl_3$ at the ratio of 1:1.5, although the IL was found to be subjected to thermal degradation involving cleavage of the alkyl chain initiated by $AlCl_3$. Lecoeur et al.[64] reported the successful synthesis of a structured Al current collector on an aluminum substrate by a template-free method, making use of a number of imidazolium-based ILs, namely, $[C_2mim][Cl]$, $[C_2mim][Tf_2N]$, $[C_8mim][Tf_2N]$, and $[C_{16}mim][Tf_2N]$, as electrolytic baths with added $AlCl_3$ as the source of Al. The nature of the cation was found to play a key role in the structuration of the aluminum deposits. For instance, deposits from $[C_8mim][Tf_2N]$, and $[C_{16}mim][Tf_2N]$ give isolated and smooth spherical agglomerates with a narrow spreading in size and distance, compared to those obtained from $[C_2mim][Tf_2N]$. Moreover, the use of cations with longer alkyl chains favored deposits with smaller or isolated entities; i.e., deposits obtained from $[C_{16}mim][Tf_2N]$-based electrolytic baths showed 2.3 μm agglomerates separated by 7.5 μm gaps, compared to the wide size distribution (diameters of 0–8 μm) of the agglomerates separated by 2.1 μm gaps for the product deposited from $[C_8mim][Tf_2N]$. To prove the positive attributes of such a structured current collector toward improving the electrode kinetics, a $Li/LiFePO_4$ cell using $LiFePO_4$ self-supported on the IL-assisted electrodeposited Al current collector was assembled and showed promising properties of capacity retention, maintaining 95% of the initial value for up to 45 cycles.

### 2.2. Metal-Air batteries

Metal–air ($O_2$) batteries, which make use of conversion reactions, noticeably Zinc–air (Zn–$O_2$) and lithium–air (Li–

  

$O_2$) batteries, are regarded as two of the most promising systems for practical high-energy applications.[69,70] A noteworthy characteristic of metal–air batteries is their open cell structure, because these batteries use oxygen from the atmosphere as their cathode material. However, to make metal–air batteries viable for commercial applications, many issues still need to be addressed, and one of the critical subjects is to develop highly efficient and low cost catalysts for the oxygen reduction reaction (ORR) on the cathode electrode. The electrochemical reactions for Zn–$O_2$ in alkaline electrolytes [Eq. (9)] and Li–$O_2$ in non-aqueous solutions [Eq. (10)] shows that the cathode electrode involves a multielectron (4 or 2 $e^-$) reduction of oxygen, which is reported to be one of the most sluggish reactions due to the overpotential during charge/discharge reactions.

$$O_2 + 2H_2O + 4e^- \rightarrow 4OH^- \quad (8)$$

$$O_2 + 2e^- + 2Li^+ \rightarrow Li_2O_2 \quad (9)$$

It is generally believed that applying effective catalysts could raise the discharge potential, drop the charge potential and ultimately improve the cyclic performance. Once again, ILs have demonstrated novelty toward the fabrication of catalysts that improve the kinetics of the ORR. Owing to their modular character, such as their electronic and steric stabilizing power, ionic nature, and high polarizability, ILs offer outstanding possibilities as media for manufacturing highly efficient electrocatalysts, such as Pt-based elemental, alloy, and multimetallic core–shell nanoparticles as well as non-Pt catalysts, e.g., oxides and functionalized high surface area carbon materials. Amongst the oxide catalysts, manganese oxides are particularly appealing candidates owing to their high catalytic activity, natural abundance, high stability, and low financial and environmental cost of manganese. Yet, their intrinsically low electrical conductivity is the main hurdle against exploiting manganese oxides as efficient ORR catalysts. The utilization of oxide nanoparticles anchored on carbon-based substrates is reported to be one approach to mitigate the inherent limitations of such oxides. Because of their chemical stability and high conductivity along with high surface area, graphene nanosheets represent an excellent substrate for hosting and growing functional nanomaterials of highly efficient electrocatalytic devices. In doing so, the introduction of the ILs moiety onto the surface of graphene oxide plays a strategic role in enhancing the electrochemical activity of the resulting hybrid nanostructure. Recently, Lee et al.[71] fabricated $Mn_3O_4$ nanoparticles integrated into electrically conductive graphene nanosheets with the aid of an IL, [(3-aminopropyl)mim][Br], through a solution-based growth mechanism. The presence of IL moieties anchored on the graphene nanosheet improved the electrocatalytic activity of the resulting hybrid nanoparticles in the oxygen reduction reaction (ORR) by a one-step–4 $e^-$ transfer pathway. The resulting graphene/$Mn_3O_4$ hybrid material was also shown to be an efficient electrocatalyst with superior activity in the Zn–$O_2$ battery. Moreover, novel catalysts such as $Mn_3O_4$/CNTs, PIL/carbon nanobubbles,[72] $CoS_2$,[73] CNTs/Pt,[74] MWCNT-supported (Au, Pt, and Pd),[75] and PtAg nanoflowers/graphene oxide[76] synthesized from ILs, have been reported to effectively improve the kinetics of ORR.

### 2.3. Na-Ion Batteries

In recent years, concerns about the sustainability of lithium supplies have prompted researchers to consider other anodic metals such as sodium (Na), which have a large abundance, low cost, easy mining of its minerals as well as the feasibility of using Al as anode current collector and in some cases aqueous electrolytes.[77] From the preparation point of view, the ionothermal fabrication route has been applied to the synthesis of electroactive materials for Na-ion batteries. Recham et al.[35] extended their successful IL-based synthetic routes for lithium-ion battery materials to the fabrication of size-controlled Na-based fluorophosphates [$Na_2MPO_4F$ ($M = Fe$, Mn, $Fe_{1-x}Mn_x$)], which are highly attractive as they are based on low cost and environmentally benign metals. Nanosized $Na_2FePO_4F$ and $Na_2MnPO_4F$ electrode materials composed of nanoparticles (~25 nm in diameter) were prepared in [$C_4$(2-$C_1$)mim][$Tf_2N$] in the temperature range of 250–280 °C, in contrast with coarse powders obtained by conventional ceramic synthesis method at much higher temperatures.[35] Electrochemical testing on $Na_2FePO_4F$ demonstrated a high capacity of 115 mA $h^{-1}$ $g^{-1}$ with lower irreversible capacity, lower polarization, and better capacity retention, compared to the samples obtained by the ceramic method.

### 2.4. Materials for Supercapacitors

Supercapacitors are devices which can store electrical energy through nonfaradaic (electrochemical double-layer capacitors (also called EDLCs); e.g., activated carbon, carbon nanotubes, graphene) and/or reversible fast faradaic (pseudocapacitors; e.g., transition metal oxides, conducting polymers) mechanisms, are newly emerging storage devices in a number of applications either complementing or replacing LIBs. This is due to their desirable properties, such as high power delivery/uptake (10–100 times higher than batteries), long cyclic lifetime (> 100 000 cycles), and low maintenance cost.

Aiming at modulating the electronic properties and enhancing the capacitive performance of EDLCs, the surface modification by doping the skeletons of carbon materials with electron-donating/withdrawing elements such as N, B, and P has recently appeared as vital alternative. For this purpose, ILs have been successfully applied in the synthesis of electrode materials for supercapacitors, serving as solvents, heteroatom source, and structure-directing agents.

Recently, Qui et al.[78] reported the preparation of N-doped mesoporous carbon materials using [$C_4$mim][$(NC)_2N$] as carbon precursor and ordered mesoporous silica as hard template. The fabricated electrodes demonstrated, in 6 M KOH aqueous electrolyte, a high specific capacitance of about 210 F $g^{-1}$ at a constant current density of 1 A $g^{-1}$, and a retention of about 95% after about 1000 cycles, demon-

  

strating the improvements ILs can offer in the development of heteroatom-doped carbon materials.

The high gravimetric capacitance of high surface area carbon based EDLCs is frequently at the expenses of their volumetric capacitance and rate capability, owing to the difficulty of balancing both surface area and tap density, simultaneously. In this regard, Guo et al.[79] took the advantage of ILs to synthesize N and B co-doped porous carbons with fully connected 3D hierarchical porosity and local graphitic texture, presenting both high gravimetric and volumetric capacitances, compared to those previously reported. The $[C_{16}mim][BF_4]$-assisted synthesis of poly(benzoxazine-co-resol)-based hierarchically porous carbon results in carbon materials with outstanding gravimetric and volumetric capacitances ($C_g \sim 247\ F\,g^{-1}$ and $C_v \sim 101\ F\,cm^{-3}$) combined with an excellent capacitance retention (96.2%) over 4000 charge/discharge cycles.

The use of graphene as electrode material is highly auspicious, but graphene nanosheets tend to stockpile when synthesized by chemical oxidation followed by reduction, a widely used method for large-scale graphene production. The aggregation of graphene nanosheets due to van der Waals interactions in turn leads to a lower specific capacitance and electrical conductivity. Once again, ILs have been applied as suitable media for the direct exfoliation of graphene sheets, thereby effectively preventing the aggregation and restacking of reduced graphene oxide, stabilized by electrostatic and cation–π interactions.[80,81] As it can be seen in Figure 6, the reduced graphene oxide (rGO) obtained from graphene in ILs can be tailored to suit a number applications, such as supercapacitors, Li–air and Li-ion batteries. The rGO/IL composite material fabricated by the addition of $[C_4mim][PF_6]$ to a graphene oxide suspension prior to the reduction procedure of rGO to graphene is a successful strategy to prevent restacking of graphene layers, resulting in a suitable material for long cycle-life energy storage devices due to its enhanced cycling properties. Composite materials obtained with a weight ratio of rGO to IL of 1:7 disclosed the highest specific capacitance of ca. $147.5\ F\,g^{-1}$ at a scan rate of $10\ mV\,s^{-1}$ in 6 M KOH electrolyte solution and excellent cycle performance with ca. 77% capacitance retention after 2000 cycles.[80] The presence of IL within rGO serves as an agent for the exfoliation of rGO, whilst enhancing the ion diffusion and charge transport, which favor the enhanced electrochemical performance.

Pseudo (or redox) capacitors, which use fast and reversible surface or near-surface reactions, possess a high specific capacitance, lessening the energy limitation of EDLCs. Anhydrous $RuO_2$ is the most widely investigated oxide for supercapacitor applications because of its superior performance. However, its practical applicability is impeded by the prohibitive cost of the starting materials and their poor safety. As a result, current research is being directed to low-cost and, sometimes, low-toxicity transition metal oxides ($Fe_2O_3$, NiO, CuO, $Co_3O_4$, and $MnO_2$). Being cheaper than $RuO_2$, environmentally benign, and easy to process with a variety of methods, efforts have been made to synthesize NiO nanostructures and films with various morphologies using high-vacuum and energy-requesting techniques such as vacuum evaporation, magnetron sputtering, or electron beam, but also more cost-effective routes such as the sonochemical, hydrothermal, and sol–gel synthesis. Recently, IL-assisted synthesis routes have been introduced as novel synthetic routes for the fabrication of transition metal nanooxides and IL/inorganic hybrids with fascinating morphologies and properties.[82–88] Mesoporous $Ni(OH)_2$ nanosheets fabricated by a sonochemical synthesis route in the presence of various ILs using nickel acetate and sodium hydroxide as starting materials resulted in the production of different forms such as nanosheets, nanorods, and nanospheres, depending on the nature of the IL employed. Subsequent calcination of the obtained $Ni(OH)_2$ material in the temperature range from 285 to 425 °C gave NiO, while preserving the original nanostructures. Mesoporous NiO nanosheets obtained in $[C_4mim][Tf_2N]$ demonstrated an exceptionally high BET surface area of $141.28\ m^2\,g^{-1}$ and excellent specific capacitance of $199.4\ F\,g^{-1}$.[84] Syntheses, making use of ILs in combination with sonochemistry, proved to be fast and easily controllable methods, avoiding the need of further templates, while resulting in a wide spectrum of morphologies ranging from nanosheets to rods and particles. Similarly, the groups of Ge[83] and Azaceta[82] reported the synthesis of NiO through the

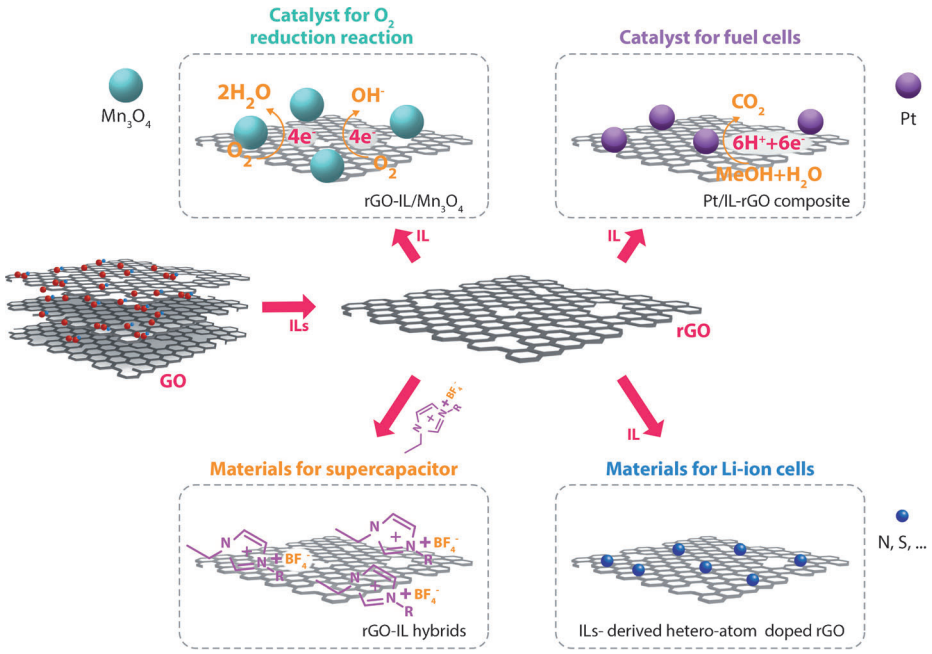


***Figure 6.*** Synthesis of reduced graphene oxide (rGO)-based materials by IL-mediated reactions of graphene oxide (GO) and their application in various fields of energy storage and conversion.

reduction of nitrates in $[C_4C_1pyr][Tf_2N]$ and a choline chloride (ChCl)/urea mixture, respectively. The use of ionic liquids for the synthesis of pseudocapacitive materials has been extended to the fabrication of varieties of conducting transition metal oxides, such as CuO,[86,87] $Co_3O_4$,[89] $MnO_2$,[85,90] etc., as thin films with different tailored morphologies and properties, demonstrating the versatility of the synthetic method.

The synthesis of conducting polymers, another class of materials for redox capacitors, has been proposed using ILs as effective growth media, resulting in significantly altered film morphologies with respect to those obtained in conventional electrolytes.[79,91–95] Poly(3,4-ethylenedioxythiophene) (PEDOT) thin films fabricated by electropolymerization in $[C_4mim][BF_4]$ showed a nearly ideal capacitive property with a specific capacitance of about $130\,F\,g^{-1}$ (in 1M $H_2SO_4$ electrolyte) and an enhanced cycle life (~70000 cycles), which is comparable to that of activated carbon materials (~$10^5$ cycles).[95] For comparison, PEDOT obtained by polymerization in 0.1 mol $L^{-1}$ $LiClO_4$/MeCN electrolyte only achieved a specific capacitance of $20\,F\,g^{-1}$ and lost its capacitance after about 1000 cycles. Similarly, ILs have been utilized for the production of different conducting polymers offering pseudocapacitive behavior, e.g., a polythiophene film in $[C_4mim][PF_6]$,[96] poly(*p*-phenylene) nanowires,[91] poly(3-methylthiophene),[92] and several others.

Tailored nanocomposite electrodes, made by combining transition metal oxides and carbon-based materials, offer increased energy density with respect to conventional EDLCs and electrical conductance and alleviate short life cycle of redox supercapacitors. Very recently, Xu et al.[88] fabricated graphite-like $C_3N_4$ hybridized $\alpha$-$Fe_2O_3$ (g-$C_3N_4$/$\alpha$-$Fe_2O_3$) hollow microspheres by a novel and eco-friendly ionothermal method. In this process, the metal-ion-containing reacting ionic liquid, $[C_4mim][FeCl_4]$, is reported to play a quadruple role as reactant, dispersing media, template, and iron source, demonstrating its key role in tuning the structure of the final hybrid composite. The g-$C_3N_4$/$\alpha$-$Fe_2O_3$ hollow microspheres surprisingly displayed the largest specific capacitance and coulombic efficiency than bare g-$C_3N_4$, $\alpha$-$Fe_2O_3$, and the g-$C_3N_4$/$\alpha$-$Fe_2O_3$ nanocomposite, affirming the potentiality of the IL-assisted synthesis of materials for high-performance supercapacitors. The superior specific capacitance of g-$C_3N_4$/$\alpha$-$Fe_2O_3$ hollow microspheres is ascribed to the peculiar structure, high BET surface area and low electronic resistance. In addition to the aforesaid electrode materials, PIL-modified graphene,[97] graphene sheets,[98] Poly(ionic liquid)-modified graphene oxide,[99] surface-modified graphene oxide,[100] free-standing carbon nanohybrid,[101] $RuO_2$ anchored on graphene and CNTs,[102] porous $Co_3O_4$,[103] and other innovative materials have been successfully synthesized in ILs.

## 3. ILs for Electrode-Processing of Energy Storage Materials

### Binders

To develop advanced electrochemical energy storage devices, both the active and inactive components need to be carefully considered. Inactive components such as binders, although necessary for the device fabrication, might strongly affect the performance along with the overall safety and environmental friendliness of the energy storage system. In LIB electrode fabrication processes, the polymer binder is responsible for binding the electrode's particles with each other, with carbon grains, and with the current collector. So far, most of the binder studies for LIBs have focused on latex suspensions such as styrene butadiene rubbers (SBR) or soluble and insoluble binders such as poly(vinylidene difluoride) (PVDF) and polytetrafluoroethylene (PTFE), respectively. However, the dimensions of the latex suspensions, which are in the range of 90 to 170 nm, can be bigger than some of the active material particles and this leads the current trend to go for nanolatex as binders.[104,105] Soluble binders such as PVDF tend to induce cracking or exfoliation from current collectors caused by contraction upon drying.[106] Antonietti and Yuan[107,108] recently reported a facile synthesis route to vinylimidazolium-type poly(ionic liquid) latexes and nanoparticles by dispersion polymerization of IL monomers in aqueous solution, claiming that these polymers, made of ionic liquid moieties, could be used as binders in lithium-ion batteries. In their pioneering work, bromide-based ILs comprising alkyl-vinylimidazolium cations (with alkyl lengths ranging from C8 to C18) were used. Surprisingly, nanoparticles of 20–40 nm were reported only with sufficiently longer alkyl chains ($\geq$ C12) when using bromide-based alkyl-vinylimidazolium ILs. Later, Paillard et al.[106] demonstrated the possibility of obtaining polymeric ionic liquid (PIL) nanoparticles from 1-vinyl-3-alkylimidazolium–TFSI monomers bearing short alkyl chains, offering a wide range of benefits, in particular as binders in combination with nanoparticle active materials for LIB applications. The electrodes obtained using the PIL nanobinder present excellent capacities, rate performance, and very good long-term cycling stability when combined with LTO and graphite-based electrodes. In general, the discovery of PIL nanolatexes opens new avenues for solving problems linked to the processing of small particles in Li-ion electrodes, such as cracking of electrodes upon drying, adhesion concerns, and the need for more binder material.

As mentioned above, fluorinated polymers such as PTFE and PVDF have been the most widely used and represent state-of-the-art binders in advanced electrochemical energy storage materials. However, both of these binders are rather expensive (ca. 20 \$ $Kg^{-1}$). Moreover, PVDF requires the use of expensive and toxic organic solvents for processing such as *N*-methyl pyrrolidone (NMP). All of the above compel the need for alternative, fluorine-free, environmentally friendly, and cheaper binders possibly allowing the use of water as the only volatile solvent in the manufacturing of electrodes. Recently, natural cellulose (NC) has been proposed as an

environmentally benign, abundant, and renewable natural polymer for replacing fluorinated polymer binders, (e.g., PVDF, PTFE), in LIB and EDLC electrodes.[104,105,109,110] Nevertheless, natural cellulose is practically insoluble in water as well as in most organic solvents and, for this reason, it is not easily processable. However, in the last few years, a solution to this issue has been found using [$C_n$mim][OAc] as a medium for slurry preparation and electrode casting. The solubilization power toward cellulose of such an ionic liquid is attributed to the ability of the C-2 hydrogen in the imidazolium core to bind with the C-1 hydroxy group of the cellulose glucose unit, resulting in the weakening of the interchain hydrogen bonds through consecutive exfoliation of the glucose fibers into fibrils, enabling an immediate dispersion in solution.[111] Making use of this peculiar action of ILs toward dissolving natural cellulose, Jeong et al.[104] showed the possibility to process volatile solvent-free slurries by dissolving cellulose in [$C_2$mim][OAc], which, after casting on the battery current collector, is diluted with water to induce a phase inversion process and thereby get fully recycled. Lithium-ion cells made with graphite and carbon-coated $LiFePO_4$ as active materials, and 1M $LiPF_6$ in EC-DEC (3:7, wt%) as electrolyte showed a specific capacity of 123 $mA\,h^{-1}\,g^{-1}$ of LFP at room temperature, asserting that the use of natural cellulose as binder opens up a new way for the development of green and low-cost electrode processing methods for LIBs. Inspired by the success of natural cellulose binders in LIBs, the groups of N. Bockenfeld[105] and A. Varzi[110] demonstrated the use of natural cellulose as binder for the development of high-performance, cheap, and environmentally friendly EDLCs. Cellulose-based EDLCs with [$C_4C_1$pyr][$Tf_2N$] electrolyte were investigated with prolonged float voltage tests at 3.7 V and offered, after 750 h, a capacitance retention of 52.7%, a much higher value than that of a state–of-the-art PVDF binder (only ~7.5%). In general, the cellulose-based electrodes fabricated using ionic liquids as solvents presented better properties than PVDF-based electrodes, in terms of morphology, porosity, and wettability. Evaluation of the aged electrodes showed that natural cellulose offers incredible chemical and mechanical stability both at high (cathode) and low (anode) voltages.

## 4. Conclusion and Outlook

Although most of the research activities have only started recently in the years 2013/2014, the tremendous potential offered by ionic liquids as advanced functional solvents, structure-directing agents, charge-compensating groups, stabilizers, and reactants (precursors) for the synthesis of energy storage devices is already apparent. Though the subject is in its infancy, the results gathered herein show the burgeoning innovative attributes of the ionothermal synthesis either in elaborating known materials/processes and/or as a novel synthesis approach enabling brand-new innovative energy materials. The syntheses of tailored materials in terms of morphology, shape, size, surface functionalization, and stabilization of metastable compounds is viable, making use of tailorable ionic liquids, whose properties and characteristics are selected by a proper combination of anions/cations.

Based on the above discussions, future work is suggested to focus on the following aspects: 1) a full-spectrum and deeper control of the interfaces between materials and ionic liquids; 2) the theoretical modeling to understand the peculiar governing reaction mechanisms of ILs in the synthesis of tailor-made electroactive materials; 3) the understanding of the templating and stabilizing mechanism of intermediate materials; and 4) the development of strategies to scale up the ionothermal synthesis process.

*We would like to acknowledge financial support of the Helmholtz association.*

Received: June 4, 2014
Published online: October 9, 2014

[1] J.-M. Tarascon, *Philos. Trans. R. Soc. London Ser. A* **2010**, *368*, 3227 – 3241.
[2] B. Dunn, H. Kamath, J.-M. Tarascon, *Science* **2011**, *334*, 928 – 935.
[3] D. R. MacFarlane, N. Tachikawa, M. Forsyth, J. M. Pringle, P. C. Howlett, G. D. Elliott, J. H. Davis, M. Watanabe, P. Simon, C. A. Angell, *Energy Environ. Sci.* **2014**, *7*, 232.
[4] M. Armand, F. Endres, D. R. MacFarlane, H. Ohno, B. Scrosati, *Nat. Mater.* **2009**, *8*, 621 – 629.
[5] G. B. Appetecchi, M. Montanino, S. Passerini, *Ion. Liq. Sci. Appl.*, American Chemical Society, Washington, DC, **2012**, pp. 4 – 67.
[6] D. Freudenmann, S. Wolf, M. Wolff, C. Feldmann, *Angew. Chem. Int. Ed.* **2011**, *50*, 11050 – 11060; *Angew. Chem.* **2011**, *123*, 11244 – 11255.
[7] T. Torimoto, T. Tsuda, K. Okazaki, S. Kuwabata, *Adv. Mater.* **2010**, *22*, 1196 – 1221.
[8] J. P. Paraknowitsch, A. Thomas, M. Antonietti, *J. Mater. Chem.* **2010**, *20*, 6746.
[9] Y. Yan, Y.-X. Yin, S. Xin, Y.-G. Guo, L.-J. Wan, *Chem. Commun.* **2012**, *48*, 10663 – 10665.
[10] H. Song, N. Li, H. Cui, C. Wang, *Nano Energy* **2014**, *4*, 81 – 87.
[11] C. Chen, X. Hu, Z. Wang, X. Xiong, P. Hu, Y. Liu, Y. Huang, *Carbon* **2014**, *69*, 302 – 310.
[12] P. Periyat, J. Colreavy, R. George, H. Hayden, M. Seery, D. E. McCormack, D. Corr, *J. Phys. Chem. C* **2007**, *111*, 1605 – 1611.
[13] V. Mansfeldova, B. Laskova, H. Krysova, M. Zukalova, L. Kavan, *Catal. Today* **2014**, *2*, 3 – 8.
[14] H. Li, S. K. Martha, R. R. Unocic, H. Luo, S. Dai, J. Qu, *J. Power Sources* **2012**, *218*, 88 – 92.
[15] C. Wessel, L. Zhao, S. Urban, R. Ostermann, I. Djerdj, B. M. Smarsly, L. Chen, Y.-S. Hu, S. Sallard, *Chemistry* **2011**, *17*, 775 – 779.
[16] M. Zukalova, M. Kalba, L. Kavan, I. Exnar, M. Graetzel, *Chem. Mater.* **2005**, *17*, 1248 – 1255.
[17] B. Scrosati, J. Hassoun, Y.-K. Sun, *Energy Environ. Sci.* **2011**, *4*, 3287.
[18] Y. Ma, G. Ji, B. Ding, J. Y. Lee, *J. Mater. Chem. A*, **2013**, *1*, 13625 – 13631.
[19] C. Gu, H. Zhang, X. Wang, J. Tu, *Mater. Res. Bull.* **2013**, *48*, 4112 – 4117.
[20] X. Meng, R. Al-Salman, J. Zhao, N. Borissenko, Y. Li, F. Endres, *Angew. Chem. Int. Ed.* **2009**, *48*, 2703 – 2707; *Angew. Chem.* **2009**, *121*, 2741 – 2745.
[21] X. Liu, J. Zhao, J. Hao, B.-L. Su, Y. Li, *J. Mater. Chem. A* **2013**, *1*, 15076.

  

[22] J. Lian, X. Duan, J. Ma, P. Peng, T. Kim, W. Zheng, *ACS Nano* **2009**, *3*, 3749 – 3761.
[23] L. Xu, J. Xia, K. Wang, L. Wang, H. Li, H. Xu, L. Huang, M. He, *Dalton Trans.* **2013**, *42*, 6468 – 6477.
[24] J. Ma, T. Wang, X. Duan, J. Lian, Z. Liu, W. Zheng, *Nanoscale* **2011**, *3*, 4372 – 4375.
[25] S. Cao, Y. Zhu, *Acta Mater.* **2009**, *57*, 2154 – 2165.
[26] J. Balach, H. Wu, F. Polzer, H. Kirmse, Q. Zhao, Z. Wei, J. Yuan, *RSC Adv.* **2013**, *3*, 7979.
[27] B. M. Bak, S.-K. Kim, H. S. Park, *Mater. Chem. Phys.* **2014**, 8 – 13.
[28] Y. Lu, C. D. Gu, X. Ge, H. Zhang, S. Huang, X. Y. Zhao, X. L. Wang, J. P. Tu, S. X. Mao, *Electrochim. Acta* **2013**, *112*, 212 – 220.
[29] Y. You, C. Gu, X. Wang, J. Tu, *J. Electrochem. Soc.* **2012**, *159*, D642 – D648.
[30] J. S. Park, J. J. Park, K. J. Kwon, H. S. Kim, C. K. Lee, *Adv. Mater. Res.* **2013**, *650*, 145 – 149.
[31] H. Zhang, L. Zeng, X. Wu, L. Lian, M. Wei, *J. Alloys Compd.* **2013**, *580*, 358 – 362.
[32] C. C. Jara, G. R. Salazar-Banda, R. S. Arratia, J. S. Campino, M. I. Aguilera, *Chem. Eng. J.* **2011**, *171*, 1253 – 1262.
[33] L. Suo, S. Sallard, Y.-S. Hu, B. Smarsly, L. Chen, *ChemElectroChem* **2014**, *1*,549 – 553.
[34] L. Zhao, Y.-S. Hu, H. Li, Z. Wang, L. Chen, *Adv. Mater.* **2011**, *23*, 1385 – 1388.
[35] N. Recham, J.-N. Chotard, L. Dupont, K. Djellab, M. Armand, J.-M. Tarascon, *J. Electrochem. Soc.* **2009**, *156*, A993.
[36] N. Recham, J.-N. Chotard, J.-C. Jumas, L. Laffont, M. Armand, J.-M. Tarascon, *Chem. Mater.* **2010**, *22*, 1142 – 1148.
[37] N. Recham, L. Dupont, M. Courty, K. Djellab, D. Larcher, M. Armand, J. Tarascon, *Chem. Mater.* **2009**, *21*, 1096 – 1107.
[38] N. Recham, M. Armand, J.-M. Tarascon, *C. R. Chim.* **2010**, *13*, 106 – 116.
[39] J.-M. Tarascon, N. Recham, M. Armand, J.-N. Chotard, P. Barpanda, W. Walker, L. Dupont, *Chem. Mater.* **2010**, *22*, 724 – 739.
[40] X. Li, Y. Liu, Z. Xiao, W. Guo, R. Zhang, *Ceram. Int.* **2014**, *40*, 289 – 296.
[41] A. Nytén, A. Abouimrane, M. Armand, T. Gustafsson, J. O. Thomas, *Electrochem. Commun.* **2005**, *7*, 156 – 160.
[42] P. Barpanda, N. Recham, J.-N. Chotard, K. Djellab, W. Walker, M. Armand, J.-M. Tarascon, *J. Mater. Chem.* **2010**, *20*, 1659.
[43] M. Ati, M. T. Sougrati, N. Recham, P. Barpanda, J.-B. Leriche, M. Courty, M. Armand, J.-C. Jumas, J.-M. Tarascon, *J. Electrochem. Soc.* **2010**, *157*, A1007.
[44] P. Barpanda, M. Ati, B. C. Melot, G. Rousse, J.-N. Chotard, M.-L. Doublet, M. T. Sougrati, S. A. Corr, J.-C. Jumas, J.-M. Tarascon, *Nat. Mater.* **2011**, *10*, 772 – 779.
[45] N. Recham, J.-N. Chotard, L. Dupont, C. Delacourt, W. Walker, M. Armand, J.-M. Tarascon, *Nat. Mater.* **2010**, *9*, 68 – 74.
[46] C. Li, L. Gu, S. Tsukimoto, P. A. van Aken, J. Maier, *Adv. Mater.* **2010**, *22*, 3650 – 3654.
[47] C. Li, L. Gu, J. Tong, J. Maier, *ACS Nano* **2011**, *5*, 2930 – 2938.
[48] B. Li, D. W. Rooney, N. Zhang, K. Sun, *ACS Appl. Mater. Interfaces* **2013**, *5*, 5057 – 5063.
[49] C. Li, C. Yin, X. Mu, J. Maier, *Chem. Mater.* **2013**, *25*, 962 – 969.
[50] Z. Gong, Y. Yang, *Energy Environ. Sci.* **2011**, *4*, 3223.
[51] X. Li, W. Guo, Y. Liu, W. He, Z. Xiao, *Electrochim. Acta* **2014**, *116*, 278 – 283.
[52] Y. Chen, J.-M. Tarascon, C. Guéry, *Electrochem. Commun.* **2011**, *13*, 673 – 676.
[53] F. Teng, M. Chen, G. Li, Y. Teng, T. Xu, S. Mho, X. Hua, *J. Power Sources* **2012**, *202*, 384 – 388.
[54] P. Barpanda, K. Djellab, N. Recham, M. Armand, J.-M. Tarascon, *J. Mater. Chem.* **2011**, *21*, 10143.
[55] R. Tripathi, G. Popov, B. L. Ellis, A. Huq, L. F. Nazar, *Energy Environ. Sci.* **2012**, *5*, 6238.
[56] Q. Wei, Q. An, D. Chen, L. Mai, S. Chen, Y. Zhao, K.-M. Hercule, L. Xu, A. Minhas-Khan, Q. Zhang, *Nano Lett.* **2014**, *14*, 1042—1048.
[57] X. Li, W. He, Z. Xiao, F. Peng, J. Chen, *J. Solid State Electrochem.* **2013**, *17*, 1991 – 2000.
[58] X. Zhang, N. Böckenfeld, F. Berkemeier, A. Balducci, *ChemSusChem* **2014**, 1 – 10.
[59] P. Barpanda, J.-N. Chotard, C. Delacourt, M. Reynaud, Y. Filinchuk, M. Armand, M. Deschamps, J.-M. Tarascon, *Angew. Chem. Int. Ed.* **2011**, *50*, 2526 – 2531; *Angew. Chem.* **2011**, *123*, 2574 – 2579.
[60] P. Barpanda, R. Dedryvère, M. Deschamps, C. Delacourt, M. Reynaud, A. Yamada, J.-M. Tarascon, *J. Solid State Electrochem.* **2012**, *16*, 1743 – 1751.
[61] S. Poetz, P. Handel, G. Fauler, B. Fuchsbichler, M. Schmuck, S. Koller, *RSC Adv.* **2014**, *4*, 6685.
[62] E. Perre, L. Nyholm, T. Gustafsson, P.-L. Taberna, P. Simon, K. Edström, *Electrochem. Commun.* **2008**, *10*, 1467 – 1470.
[63] G. Oltean, L. Nyholm, K. Edström, *Electrochim. Acta* **2011**, *56*, 3203 – 3208.
[64] C. Lecoeur, J.-M. Tarascon, C. Guery, *J. Electrochem. Soc.* **2010**, *157*, A641.
[65] K. Edström, D. Brandell, T. Gustafsson, L. Nyholm, *Electrochem. Soc. Interface* **2011**, *20*, 41 – 46.
[66] L. Hu, F. La Mantia, H. Wu, X. Xie, J. McDonough, M. Pasta, Y. Cui, *Adv. Energy Mater.* **2011**, *1*, 1012 – 1017.
[67] K. Ziegler, H. Lehmkhul, *Z. Anorg. Allg. Chem.* **1956**, *283*, 414 – 424.
[68] W. Kautek, S. Birkle, *Electrochim. Acta* **1989**, *34*, 1213 – 1218.
[69] J. S. Lee, S. T. Kim, R. Cao, N.-S. Choi, K. T. Lee, J. Cho, *Adv. Energy Mater.* **2011**, *1*, 34 – 50.
[70] Y. Li, M. Gong, Y. Liang, J. Feng, J.-E. Kim, H. Wang, G. Hong, B. Zhang, H. Dai, *Nat. Commun.* **2013**, *4*, 1805.
[71] J.-S. Lee, T. Lee, H.-K. Song, J. Cho, B.-S. Kim, *Energy Environ. Sci.* **2011**, *4*, 4148.
[72] S. Soll, T.-P. Fellinger, X. Wang, Q. Zhao, M. Antonietti, J. Yuan, *Small* **2013**, *9*, 4135 – 4141.
[73] C. Zhao, D. Li, Y. Feng, *J. Mater. Chem. A* **2013**, *1*, 5741.
[74] S. Guo, S. Dong, E. Wang, *Adv. Mater.* **2010**, *22*, 1269 – 1272.
[75] D. V. K. D. Sara, M. Shamsipur, A. Rouhollahi, *Adv. Mater. Res.* **2013**, *829*, 589 – 593.
[76] J.-J. Lv, J.-X. Feng, S.-S. Li, Y.-Y. Wang, A.-J. Wang, Q.-L. Zhang, J.-R. Chen, J.-J. Feng, *Electrochim. Acta* **2014**, *133*, 407—413.
[77] L. G. Chagas, D. Buchholz, L. Wu, B. Vortmann, S. Passerini, *J. Power Sources* **2014**, *247*, 377 – 383.
[78] B. Qiu, C. Pan, W. Qian, Y. Peng, L. Qiu, F. Yan, *J. Mater. Chem. A* **2013**, *1*, 6373.
[79] D.-C. Guo, J. Mi, G.-P. Hao, W. Dong, G. Xiong, W.-C. Li, A.-H. Lu, *Energy Environ. Sci.* **2013**, *6*, 652.
[80] J. Kim, S. Kim, *Appl. Surf. Sci.* **2014**, 1 – 7.
[81] J. Kim, S. Kim, *Electrochim. Acta* **2014**, *119*, 11 – 15.
[82] E. Azaceta, N. T. Tuyen, D. F. Pickup, C. Rogero, J. E. Ortega, O. Miguel, H.-J. Grande, R. Tena-Zaera, *Electrochim. Acta* **2013**, *96*, 261 – 267.
[83] X. Ge, C. D. Gu, Y. Lu, X. L. Wang, J. P. Tu, *J. Mater. Chem. A* **2013**, *1*, 13454.
[84] T. Alammar, O. Shekhah, J. Wohlgemuth, A.-V. Mudring, *J. Mater. Chem.* **2012**, *22*, 18252.
[85] J.-K. Chang, C.-H. Huang, W.-T. Tsai, M.-J. Deng, I.-W. Sun, P.-Y. Chen, *Electrochim. Acta* **2008**, *53*, 4447 – 4453.
[86] J. S. Shaikh, R. C. Pawar, R. S. Devan, Y. R. Ma, P. P. Salvi, S. S. Kolekar, P. S. Patil, *Electrochim. Acta* **2011**, *56*, 2127 – 2134.
[87] L. Xu, J. Xia, K. Wang, H. Li, L. Huang, Z. Luo, L. Wang, *Eur. J. Inorg. Chem.* **2013**, 2315 – 2323.

[88] L. Xu, J. Xia, H. Xu, S. Yin, K. Wang, L. Huang, L. Wang, H. Li, *J. Power Sources* **2014**, *245*, 866 – 874.
[89] B. G. Choi, M. Yang, S. C. Jung, K. G. Lee, J.-G. Kim, H. Park, T. J. Park, S. B. Lee, Y.-K. Han, Y. S. Huh, *ACS Nano* **2013**, *7*, 2453 – 2460.
[90] J.-K. Chang, C.-H. Huang, W.-T. Tsai, M.-J. Deng, I.-W. Sun, *J. Power Sources* **2008**, *179*, 435 – 440.
[91] M. Al Zoubi, F. Endres, *Electrochim. Acta* **2011**, *56*, 5872 – 5876.
[92] M. Biso, M. Mastragostino, M. Montanino, S. Passerini, F. Soavi, *Electrochim. Acta* **2008**, *53*, 7967 – 7971.
[93] T. Carstens, A. Prowald, S. Z. El Abedin, F. Endres, *J. Solid State Electrochem.* **2012**, *16*, 3479 – 3485.
[94] D. He, Y. Guo, Z. Zhou, S. Xia, X. Xie, R. Yang, *Electrochem. Commun.* **2009**, *11*, 1671 – 1674.
[95] K. Liu, Z. Hu, R. Xue, J. Zhang, J. Zhu, *J. Power Sources* **2008**, *179*, 858 – 862.
[96] H. Zhang, L. Hu, J. Tu, S. Jiao, *Electrochim. Acta* **2014**, *120*, 122 – 127.
[97] J. P. C. Trigueiro, R. L. Lavall, G. G. Silva, *J. Power Sources* **2014**, *256*, 264 – 273.
[98] J. Yan, Y. Xiao, G. Ning, T. Wei, Z. Fan, *RSC Adv.* **2013**, *3*, 2566.
[99] T. Y. Kim, H. W. Lee, M. Stoller, D. R. Dreyer, C. W. Bielawski, R. S. Ruoff, K. S. Suh, *ACS Nano.* **2011**, *5*, 436 – 442.
[100] J. Kim, S. Kim, *Appl. Surf. Sci.* **2014**, *295*, 31 – 37.
[101] L. Wei, W. Jiang, Y. Yuan, K. Goh, D. Yu, L. Wang, Y. Chen, *J. Solid State Chem.* **2014**, 1 – 7.
[102] W. Wang, S. Guo, I. Lee, K. Ahmed, J. Zhong, Z. Favors, F. Zaera, M. Ozkan, C. S. Ozkan, *Sci. Rep.* **2014**, *4*, 4452.
[103] W. Liu, L. Xu, D. Jiang, J. Qian, Q. Liu, X. Yang, K. Wang, *CrystEngComm* **2014**, *16*, 2395.
[104] S. S. Jeong, N. Böckenfeld, A. Balducci, M. Winter, S. Passerini, *J. Power Sources* **2012**, *199*, 331 – 335.
[105] N. Böckenfeld, S. S. Jeong, M. Winter, S. Passerini, A. Balducci, *J. Power Sources* **2013**, *221*, 14 – 20.
[106] J. von Zamory, M. Bedu, S. Fantini, S. Passerini, E. Paillard, *J. Power Sources* **2013**, *240*, 745 – 752.
[107] J. Yuan, M. Antonietti, *Polymer* **2011**, *52*, 1469 – 1482.
[108] J. Yuan, M. Antonietti, *Macromolecules* **2011**, *44*, 744 – 750.
[109] A. Brandt, S. Pohlmann, A. Varzi, A. Balducci, S. Passerini, *MRS Bull.* **2013**, *38*, 554 – 559.
[110] A. Varzi, A. Balducci, S. Passerini, *J. Electrochem. Soc.* **2014**, *161*, A368 – A375.
[111] T. Heinze, S. Dorn, M. Schöbitz, T. Liebert, S. Köhler, F. Meister, *Macromol. Symp.* **2008**, *262*, 8 – 22.